

Identification of Repeating Earthquakes: Misconception of Waveform Similarity and a Physics-based Solution

Dawei Gao¹ and Honn Kao²

¹University of Victoria

²Geological Survey of Canada

November 23, 2022

Abstract

Identification of repeating earthquakes (repeaters) usually depends on waveform similarity expressed as the corresponding cross-correlation coefficient (CC) above a prescribed threshold, typically ranging from 0.70 to 0.98. However, the robustness and effectiveness of such a strategy have never been thoroughly examined. In this study, we examine whether CC is a valid proxy for repeater identification through both synthetic and real earthquake experiments. We reveal that CC is controlled by not only the inter-event distance but also many other factors, including station azimuth, epicentral distance, velocity structure, etc. Consequently, CC lacks the resolution in identifying true repeaters. We propose a physics-based approach that considers both inter-event separation and rupture radius. For an event pair to be true repeaters, their inter-event separation must be smaller than the rupture radius of the larger event. Our results imply that a systematic recheck of previously identified repeaters and associated interpretations/hypotheses may be important and necessary.

1 **Identification of Repeating Earthquakes:**
2 **Misconception of Waveform Similarity and a Physics-based Solution**

3 **Dawei Gao^{1,2} and Honn Kao^{1,2*}**

4 ¹School of Earth and Ocean Sciences, University of Victoria, Victoria, British Columbia,
5 Canada.

6 ²Pacific Geoscience Centre, Geological Survey of Canada, Sidney, British Columbia, Canada.

7
8 Corresponding author: Honn Kao (honn.kao@canada.ca)

9
10 **Key Points:**

- 11 • There is no simple relationship between cross-correlation coefficient (CC) and inter-event
12 separation.
- 13 • CC is affected by many factors and thus lacks the resolution to determine two events as
14 true repeating or just neighboring earthquakes.
- 15 • To reliably identify repeating earthquakes, we should rely on the precise estimation of
16 both rupture radius and inter-event separation.
17

18 **Abstract**

19 Identification of repeating earthquakes (repeaters) usually depends on waveform similarity
20 expressed as the corresponding cross-correlation coefficient (CC) above a prescribed threshold,
21 typically ranging from 0.70 to 0.98. However, the robustness and effectiveness of such a strategy
22 have never been thoroughly examined. In this study, we examine whether CC is a valid proxy for
23 repeater identification through both synthetic and real earthquake experiments. We reveal that
24 CC is controlled by not only the inter-event distance but also many other factors, including
25 station azimuth, epicentral distance, velocity structure, etc. Consequently, CC lacks the
26 resolution in identifying true repeaters. We propose a physics-based approach that considers both
27 inter-event separation and rupture radius. For an event pair to be true repeaters, their inter-event
28 separation must be smaller than the rupture radius of the larger event. Our results imply that a
29 systematic recheck of previously identified repeaters and associated interpretations/hypotheses
30 may be important and necessary.

31

32 **Plain Language Summary**

33 Repeating earthquakes (repeaters) are events that occur repeatedly on the same fault patch with
34 nearly identical waveforms. They provide important insights into a variety of geophysical
35 subjects such as fault behavior, subsurface structure change, inner core rotation, and nucleation
36 process of earthquake and landslide. The identification of repeaters is usually solely based on
37 waveform similarity, but the criteria can vary significantly from one case to another. With both
38 synthetic and real data, we find that waveform similarity is controlled by many factors, in
39 addition to inter-event distance. Therefore, a higher degree of waveform similarity does not
40 necessarily imply a smaller hypocenter separation, and vice versa. Our results undoubtedly
41 suggest that waveform similarity alone is insufficient to reliably identify true repeaters. We
42 propose a physics-based approach that considers both inter-event separation and earthquake
43 source dimension. For an event pair to be true repeaters, their inter-event separation must be
44 smaller than the rupture radius of the larger event. Our results imply that previously identified
45 repeaters and associated interpretations/hypotheses may be unreliable and hence need a
46 systematic reexamination.

47

48 **1. Introduction**

49 Repeating earthquakes (repeaters) are events that recurrently rupture the same fault patch with
50 the same focal mechanisms, often characterized by nearly identical waveforms (Uchida and
51 Bürgmann, 2019). These events are of great importance in many aspects of geophysics, such as
52 monitoring subtle temporal changes of crustal properties (e.g., Poupinet et al., 1984; Schaff and
53 Beroza, 2004; Sawazaki et al., 2015; Pacheco et al., 2017) and oceanic temperature (Wu et al.,
54 2020), estimating fault creep (e.g., Nadeau and Johnson, 1998; Uchida et al., 2003, 2006;
55 Matsubara et al., 2005; Yu, 2013; Materna et al., 2018), investigating inner core rotation (e.g., Li
56 and Richards, 2003; Zhang et al., 2005, 2008; Tkalčić et al., 2013), evaluating the precision of
57 earthquake locations (e.g., Li and Richards, 2003; Meier et al., 2004; Schaff and Richards, 2011;
58 Jiang et al., 2014), and providing insights into the nucleation process of earthquakes (Kato et al.,
59 2012; Kato and Nakagawa, 2014; Meng et al., 2015; Huang and Meng, 2018) and landslides
60 (Yamada et al., 2016).

61 Over the past few decades, repeaters are reported world-wide, in both tectonic and
62 nontectonic settings (Uchida and Bürgmann, 2019). The most commonly used scheme for
63 identifying repeaters is to examine waveform similarity by setting a threshold in the value of
64 cross-correlation coefficient (CC) between a waveform pair. The employed CC threshold is
65 somewhat arbitrary depending on the available data, ranging in 0.70–0.90 for regions with sparse
66 network coverage (usually with one channel/station), and 0.90–0.98 for areas with denser
67 instrumentation (usually using a minimum of two channels/stations, Table S1). With the
68 increasing computing power, detecting repeaters through waveform similarity has become a
69 routine process in seismology (e.g., Hotovec-Ellis and Jeffries, 2016; Tepp, 2018; Chamberlain
70 et al., 2018). However, to our best knowledge, the robustness and effectiveness of this classical
71 strategy have never been thoroughly examined. In early times, the lack of examination was
72 largely due to limited data availability (especially near-field observations) and/or poor waveform
73 quality. As the number of seismograph stations increases rapidly in recent years, such data
74 constraints no longer exist. Yet, many recent studies simply follow the conventional approach
75 without questioning the original assumption (Table S1).

76 The focus of this study, therefore, is to investigate whether waveform similarity is a valid
77 proxy for repeater identification. We first examine how the CC varies with inter-event separation
78 and uncover the overlooked factors through a large number of synthetic experiments. We then
79 illustrate that waveform similarity indeed lacks the resolution to determine whether two events
80 are true repeaters or not using a dense local borehole array data in Parkfield, California. To more
81 reliably identify repeating earthquakes, we propose a physics-based approach that considers both
82 inter-event separation and the rupture areas. We validate our approach using events occurred in
83 the Fox Creek area, Alberta, Canada, where earthquake source parameters are well constrained
84 by local stations.

85

86 **2. Synthetic Experiments**

87 Figure 1a illustrates the configuration of our synthetic experiments. We place one event (the
88 template event) at the centre of an array. Then we incrementally shift the other event (the
89 matched event) with the same focal mechanism in either north-south (Figure 1a) or vertical
90 direction (Figure 1b). The technical details of our experiment setup and CC calculation are
91 presented in the Supporting Information (Texts S1 and S2).

92

93 **2.1 Constraining Inter-event Separation Using Single-channel Data**

94 Single-channel CC has been used in numerous previous studies to infer the existence of
95 repeaters (Table S1), thus we first examine how the CC varies with source separation using
96 single-channel (i.e., E, N, or Z) data. In Figure 2a and 2b, we present the results of a
97 representative case, namely, a strike-slip earthquake (template event) at the depth of 3 km with a
98 station 5 km away from the epicenter.

99 For horizontal inter-event separation, our results indicate that single-channel waveforms can
100 have very different sensitivities (Figure 2a). In general, the CC value decreases with increasing
101 hypocentral separation. It quickly drops from 1 when the two sources are perfectly co-located to
102 <0.5 when the pair is ~ 1 km apart. Beyond that, the CC curves appear to fluctuate between 0.2
103 and 0.4 without a clear monotonic trend. This implies that using the CC value to constrain the

104 difference between two nearby hypocenters may not be ideal once the separation is on the order
 105 of kilometers.

106 Another important point in Figure 2a is that the CC value may be strongly affected by the
 107 combined effect of focal mechanism and relative position between the source and station. This
 108 effect is best illustrated by Station 3 as the inter-event distance increases. For all 3 channels, the
 109 CC value decreases when the matched event shifts northward from 0 to -1.3 km. Once passing
 110 the -1.3 km mark, the CC value has a sudden drop on both E and Z channels but continues to
 111 increase on the N channel. This unexpected result happens when Station 3 is located very close
 112 to one of the assumed nodal planes (Figure 1a). As the matched event shifts northward, Station
 113 3's position moves across the nodal plane and therefore causes polarity reversal on the Z and E
 114 channels. When the inter-event separation reaches -2.6 km, Station 3 is nearly of equal distance
 115 to both the template and matched events (Figure 1a), leading to identical waveforms on the N
 116 channel but reversed shapes on the other two channels (Figure S1). Consequently, the final
 117 (maximum) CC values would be 1 for the N channel (taken when the two P phases coincide) and
 118 ~ 0.5 – 0.6 for the Z and E channels (taken when the two P phases are offset by half a cycle), even
 119 though the two events are 2.6 km apart. We have tested other types of focal mechanisms (pure
 120 normal or thrust-faulting) and the profound effect remains (Figure S2).

121 Unlike the cases of horizontal separation, the CC curves obtained with different channels and
 122 stations overall show similar trends when the two sources are vertically apart (Figure 2b), hinting
 123 that using the CC value to constrain the vertical inter-event separation is probably independent of
 124 data channel and station azimuth. Especially for the vertical channel, stations with different
 125 azimuths can have identical sensitivities to the inter-event separation when the focal mechanism
 126 is pure strike-slip (Figure 2b, right panel). Notice that the CC curves derived from the E and N
 127 channels of Station 1 are identical to those from the N and E channels of Station 3, respectively
 128 (Figure 2b), due to the symmetrical station location on the focal sphere (Figure 1a). Results of
 129 these tests once again suggest that a larger CC does not necessarily represent a larger separation
 130 once the vertical separation exceeds a certain threshold (~ 0.5 km). We also find that results from
 131 different focal mechanisms are comparable (Figure S2). Last but not the least, the CC value
 132 generally drops much faster with increasing vertical source separation (Figure 2a vs. 2b) as a
 133 result of more minor discrepancies between waveforms. In other words, the CC seems to be
 134 much more sensitive to capture the vertical source shift than the horizontal.

135 The simple tests above demonstrate that, in addition to inter-event distance, CC can be
 136 severely affected by the specific channel used, combined effect of focal mechanism and relative
 137 position between the source and station, and source separation direction (horizontal vs. vertical).

138

139 **2.2 Constraining Inter-event Separation Using Single-station (3-channel) Data**

140 If data from all three channels are included, we find that the CC sensitivity to source
 141 separation increases dramatically for the cases of horizontal separation (e.g., Figures 2a vs. S3a)
 142 but insignificantly for those of vertical separation (e.g., Figures 2b vs. S4a). For a given
 143 horizontal separation, Stations 1 and 3 tend to have the lowest and highest CC values,
 144 respectively (Figures 2c and S3), strongly suggesting that station azimuth is an important factor
 145 that cannot be overlooked. In contrast, the influences of focal depth, epicentral distance, and
 146 source focal mechanisms seem to be limited (Figure S3). Our results indicate that a station

147 approximately in line with the template and matched events can be more effective in delineating
148 the inter-event separation (e.g., Station 1 in our case, Figure 1a).

149 The computed CC overall is very sensitive to vertical inter-event separation with the only
150 exception when the source is deep and the station is close (e.g., $D=10$ km and $R=5$ km, Figures
151 2d and S4). For a close station ($R=5$ km) and a shallow source ($D=3$ km), even a very small (0.2
152 km) vertical separation can lead to a dramatic drop of CC to <0.8 (Figure S4a and S4c), but the
153 sensitivity gets worse when the source is deeper (Figure S4b and S4d). This is mainly a velocity
154 structure effect caused by smaller seismic velocity variation at deep depths. In other words, the
155 CC sensitivity would become higher when the corresponding velocity structure (and therefore
156 the observed waveforms) are more complicated. An important observation to point out is that the
157 CC is very sensitive to vertical inter-event separations when the epicentral distance is large (e.g.,
158 $R = 50$ or 150 km), regardless of the focal depth (Figure S4e-l). This is opposite to what is
159 expected for earthquake depth determination as seismic phase arrival times at distant stations
160 usually have less depth constraint. It turns out that waveforms at distant stations can have better
161 developed depth phases (i.e., seismic phases reflected from either the free surface or Moho).
162 Consequently, a subtle change of source depth may lead to a significant waveform difference and
163 therefore an apparent CC drop.

164 Therefore, our experiments in this section further demonstrate that CC can be affected by the
165 number of channels used, station azimuth, velocity structure, and epicentral distance.

166

167 **2.3 Constraining Inter-event Separation Using Multi-station Data**

168 For areas with excellent network coverage, it is common to use a minimum of two stations
169 (usually only the vertical channel) for identifying repeaters (Table S1). The majority of prior
170 work (Table S1) calculate CC separately for each station. This approach essentially uses more
171 stations with different azimuths and/or epicentral distances but may not necessarily improve the
172 sensitivity if all available stations happen to be the ones with lower sensitivities (Figure 2c and
173 2d). An alternative way is to calculate the CC simultaneously across the network (e.g., Yao et al.,
174 2017) which includes the constraint of traveltime moveout. In such a case, the computed CC can
175 be extremely sensitive to hypocentre difference (Gao and Kao, 2020). We refrain from
176 investigating the multi-station scenario as the CC sensitivity is known to be strongly affected by
177 network geometry (Chamberlain and Townend, 2018; Gao and Kao, 2020), and thus no
178 general/common rules can be inferred objectively.

179 In summary, our synthetic experiments reveal that CC is a very complex function of many
180 aforementioned factors. A higher CC value does not necessarily represent a smaller inter-event
181 separation, and vice versa. Therefore, in contrast to the conventional wisdom, our synthetic
182 results indicate that CC is not a robust indicator of two events being true repeaters or not.

183

184 **3. Verification With Real Earthquake Examples**

185 The High-Resolution Seismic Network (HRSN, Figure 3a) is a dense local array of borehole
186 seismometers deployed in the Parkfield area, California, and operated by the Berkeley
187 Seismological Laboratory. The HRSN waveform data generally have exceptionally high signal-
188 to-noise ratio (SRN) and hence are ideal for the purpose of this study to verify whether

189 waveform similarity is a good proxy of repeater identification. Here we take three events (No. 1-
190 3, Figure 3a) from two well studied repeating earthquake clusters in Parkfield (Abercrombie,
191 2014). Among them, events No. 1 and 3 belong to the same cluster with similar source areas
192 while event No. 2 occurred on a different fault patch.

193

194 **3.1 CC between Non-repeaters**

195 We first calculate the CC between non-repeaters, i.e., No. 1 and 2. We only use data from
196 stations nearly free from noise contamination, as hinted by the flat waveforms before the P wave
197 arrival (one example is shown in Figure 3b). The most striking result of our analysis is that the
198 CC derived from unfiltered 3-channel waveforms indeed differ significantly among different
199 stations, ranging from 0.76 to just above 0.95 (Figure 3c). Such a wide CC range is consistent
200 with the inference from our synthetic tests that the CC can be severely affected by station
201 azimuth and/or source-receiver position/path even under the noise-free circumstances.
202 Additionally, the CC may be further affected by local structures of velocity discontinuities as this
203 region is featured by complex fault zones (Figure 3a). Our study reveals that the waveforms of
204 non-repeaters can show apparent difference (top panel in Figure 3b), slight difference (middle
205 panel in Figure 3b) or little difference (bottom panel in Figure 3b) at different stations. For any
206 given station, the CC values of different channels can be either similar or different (Figure S5).
207 Together, waveform similarity indeed lacks the resolution to decide the two events to be
208 repeaters or not.

209 Because nearly all prior works practically identify repeaters through filtered waveforms for
210 the purpose of mitigating the noise impact, we then examine the effects of commonly used band-
211 pass filters (Table S2). Our results indicate that the CC obtained from different stations all show
212 a clear increasing trend when the passband becomes narrower (Figures 3c and S5). Especially for
213 the very narrow but very popular 1-4 Hz band-pass filter used by many previous studies (Table
214 S2), 9 out of 10 stations have $CC > 0.98$ (Figure 3c), which is the highest CC threshold used in
215 the literature in selecting repeaters (Table S1). This simple experiment highlights the overlooked
216 fact that filtering could remove the important frequency content in the signal that distinguishes
217 the physical separation of the two events, in addition to reducing the unwanted noise. For
218 example, even a very wide band-pass filter (1-20 Hz) would remove the very high frequency
219 signal with poor similarity and thus lead to very similar waveforms as shown in Figure 3d. What
220 makes it worse is that filtering would change both the shape and width of the P wave and
221 therefore make the subtle difference in the S-P differential traveltime (0.012s in Figure 3d)
222 unresolvable, effectively throwing away the most critical information on the relative distance
223 between the two sources. The results here strongly imply that filtering would lead to
224 misidentification of repeaters if the selection criterion is solely based on waveform similarity.
225 We also tested the effect of template window length (T_{win}) associated with different filters
226 (Table S2) in calculating CC (Text S2) and the results are comparable (Figure S6). Two
227 examples of how filtering increases the waveform similarity at close and distant stations,
228 respectively, are presented in Figures S7 and S8 for reference.

229

230 **3.2 CC between True Repeaters**

231 Interestingly, we also find that, for true repeaters like events No. 1 and 3, the CC value
 232 obtained from different stations still differ significantly from each other (Figure S9). The
 233 unfiltered waveforms can be nearly identical at one station (Figure S10a) but also can be of
 234 minor difference at another station even with nearly no noise (zoom-in box in Figure S10b).
 235 Without noise contamination, the waveform difference between true repeaters may arise from the
 236 variability of the rupture process (such as the slight difference in earthquake initiation point)
 237 (Uchida, 2019) and/or seismic velocity change (e.g., Poupinet et al., 1984; Sawazaki et al., 2015;
 238 Pacheco et al., 2017). With the band-pass filters applied, the waveform discrepancy overall
 239 becomes much smaller as indicated by the increasing CC values (Figure S9). This is similar to,
 240 but less dramatic as, the case of non-repeaters.

241 Taken together, non-repeaters indeed can have very similar waveforms (bottom panel in
 242 Figure 3b) while the waveforms of true repeaters may display minor difference (Figure S10b). In
 243 contrast to the traditional view, our observations undoubtedly suggest that waveform similarity is
 244 not a good proxy for repeater identification, especially with band-pass filters applied.

245

246 4. A Physics-based Solution

247 Although waveform similarity can be useful in recognizing potential repeaters (e.g., Sáez et
 248 al., 2019), the most fundamental concern of two events being repeaters or not is whether their
 249 ruptures significantly overlap with each other. In case of two events rupturing the same fault
 250 patch but from different nucleation points, they should be deemed repeaters even though the
 251 corresponding waveform similarity may not be perfect (Uchida, 2019). Therefore, a physics-
 252 based approach considering both inter-event separation and the source rupture areas should be
 253 the most reasonable solution. Specifically, we define two events to be repeaters if their inter-
 254 event distance is no larger than the source dimension of the bigger event. In other words, the
 255 hypocenter of the smaller event must fall within the rupture area of the bigger event.

256 There are different ways in seismology to characterize the rupture area of an earthquake
 257 source (Stein and Wysession, 2009). One of the most common, and perhaps the easiest, method
 258 is to estimate the equivalent rupture radius (ERR), which is defined as the radius of a circle
 259 whose area is the same as the source rupture area. The ERR can be estimated from the event's
 260 stress drop ($\Delta\sigma$) via the well-established circular dislocation model (Brune, 1970):

$$261 \quad ERR = \sqrt[3]{\frac{7M_o}{16 \Delta\sigma}} \quad (1)$$

262 where M_o is the event's scalar seismic moment. The $\Delta\sigma$ value can either be reasonably assumed
 263 (Table S3) or directly derived (e.g., Abercrombie, 2014; Ellsworth and Bulut, 2018).

264 For the distance of inter-event separation, however, it is always a challenge to get a precise
 265 measurement unless a very dense local array is available (Cheng et al., 2007). In case of limited
 266 data, we propose a variant of the double difference method (HypoDD; Waldhauser and
 267 Ellsworth, 2000) that minimizes the residual between observed and predicted relative S-P
 268 differential traveltimes through three-dimensional (3D) grid search to precisely estimate the inter-
 269 event distance. We explain the detail of our method, named the differential traveltimes double-
 270 difference (DTDD) method, in the Supporting Information (Text S3).

271 Figure 4 presents an example of using the DTDD method to determine the precise relative
 272 position of three events with similar waveforms recorded at 4 nearby stations in Fox Creek,
 273 Alberta, Canada. Among them, events No. 4 and 6 are found to be ~ 200 m apart, consistent with
 274 the subtle difference in S-P time (left yellow zoom-in window in Figure 4b). In comparison,
 275 events No. 5 and 6 are effectively co-located (Figures 4c and S11) as indicated by the identical
 276 S-P time at all four stations (right yellow zoom-in window in Figure 4b). The corresponding
 277 ERRs of these three events are 60 (No. 4), 31 (No. 5), and 70 (No. 6) m, respectively. Therefore,
 278 we conclude that events No. 5 and No. 6 are true repeating events (i.e., $\text{ERR} > \text{inter-event}$
 279 distance), whereas events No. 4 and No. 6 are at most neighboring events ($\text{ERR} < \text{inter-event}$
 280 distance).

281 We finally note that both event pairs have high CC values (0.83 between events No. 4 and 6,
 282 0.88 between events No. 5 and 6; Figure 4b). Consequently, the determination of these event
 283 pairs being true repeaters or not can be arbitrary depending on the choice of the CC threshold
 284 (e.g., the choice of 0.80, 0.85, or 0.90 will lead to completely different outcomes). Our results
 285 clearly indicate that the CC can drop below 0.9 even for true repeating events when the
 286 waveforms of the smaller event are contaminated with noise (event No. 5; Figure 4b). It further
 287 underscores the challenge in identifying repeaters based solely on waveform similarity with the
 288 presence of noise.

289

290 5. Discussion

291 There are two key parameters, i.e., ERR and inter-event distance, in our proposed framework
 292 of identifying repeaters. To uniquely estimate the ERR of a small event, it is necessary to specify
 293 the value of $\Delta\sigma$ in the popular Brune model (Equation 1). While most previous studies consider
 294 $\Delta\sigma$ to be no more than 10 MPa (Table S3), detailed analysis of dense local borehole array data in
 295 the Parkfield area suggests that $\Delta\sigma$ of small ($M_L \sim 2$) events can be as high as tens of MPa
 296 (Abercrombie, 2014). Since a smaller $\Delta\sigma$ value will yield a larger ERR, underestimation of $\Delta\sigma$ is
 297 likely to misclassify neighboring events as repeaters, and vice versa. Therefore, the uncertainty
 298 due to a poorly constrained (or wrongly assumed) $\Delta\sigma$ value should be treated with caution.

299 The DTDD method that we develop to estimate the inter-event distance with limited
 300 waveform data relies on precise measurement of the S-P differential traveltime (Text S3). For a
 301 typical crustal model (i.e., $V_p = 6.5$ km/s and $V_p/V_s = 1.73$), a 0.01s difference in the S-P time
 302 corresponds to a hypocentral difference of ~ 90 m (Hayward and Bostock, 2017). Consequently
 303 we need to pay attention to two potential issues. First, the application of digital filtering, such as
 304 the band-pass filters used in previous studies, may change the width of P wave, leading to a
 305 slight shift between the P and S phases (one example is shown in Figure 3d). The small bias
 306 (0.012 s in the case shown in Figure 3d) is equivalent to a mislocation of ~ 100 m that is
 307 sufficient to cause misinterpretation for events with small source dimension. Therefore, we
 308 prefer to use unfiltered broadband waveforms in the measurement of S-P differential traveltime
 309 to avoid any possible bias from waveform filtering.

310 The second issue is the resolution limit defined by the sampling rate of waveform data. It can
 311 be particularly problematic if the original sampling rate is less than 100 Hz (i.e., ≥ 0.01 s between
 312 samples) so the hypocentral uncertainty becomes comparable to the source dimension of small
 313 events. A straightforward solution is to pre-process waveforms with interpolation to increase its

314 apparent sampling rate before measuring the S-P times (Li et al., 2007, 2011). Similarly, the grid
315 size used in the DTDD source-searching process should be much smaller than the source
316 dimension of the targeted events to achieve optimal spatial resolution.

317 We note that, in the extreme case of limited data from only one or two stations, the DTDD
318 solution can be highly non-unique. Consequently, a priori constraints must be introduced to
319 quantitatively estimate the inter-event distance. One commonly adopted remedy is to require the
320 two events to occur on a given fault plane (e.g., Li et al., 2007). Another commonly adopted
321 constraint comes from the ambient tectonic loading rate, i.e., the recurrence interval between two
322 repeaters should be proportional to the size of the second event (e.g., Li et al., 2007, 2011;
323 Bohnhoff et al., 2017). If the two events occur very closely to each other in time, they are more
324 likely to be neighboring events because the fault patch ruptured during the first event has not
325 healed yet.

326

327 **6. Conclusion**

328 In this study we reveal that CC can be severely affected by many factors, including the choice
329 of one specific channel or all three channels, combined effect of focal mechanism and relative
330 position between the source and station, station azimuth, epicentral distance, velocity structure,
331 orientation of the source separation (horizontal vs. vertical), network geometry, and the filter's
332 frequency bandwidth. In reality, noise, heterogeneity in the crust, and variation in the Moho
333 depth may further contribute to the complication of CC sensitivity. Therefore it is almost
334 impossible to reliably identify repeaters solely based on a given CC value, implying that a
335 systematic recheck of previously identified repeaters and associated interpretations/hypotheses
336 may be important and necessary.

337 To more reliably identify true repeaters, we propose a physics-based approach that considers
338 both ERR and inter-event separation. For an event pair to be true repeaters, their inter-event
339 separation must be no larger than the ERR of the larger event. For the precise estimation of inter-
340 event distance in case of limited data, we develop the DTDD method which relies on the relative
341 S-P differential traveltime. Finally we illustrate the effectiveness of the DTDD method and
342 validate the physics-based approach in selecting repeaters using earthquakes occurred in the Fox
343 Creek area, Alberta, Canada. The findings of this work has far-reaching impact on not only
344 repeating earthquake research but also other waveform-similarity-based studies.

345

346

347 **Acknowledgements**

348 We are grateful to Lupei Zhu for providing the FK code that is used in generating synthetic
349 seismograms. We specially thank Bei Wang for helping calculate the stress drops of the Fox
350 Creek events, and thank Didem Cambaz and Edwin Nissen for the help offered in this study.
351 Insightful discussions with Toshihiro Igarashi, Naoki Uchida, David P. Schaff, Makoto Naoi,
352 Jianlong Yuan, Stan Dasso, Kelin Wang, Ryan Visser, Rachel E. Abercrombie, Fengzhou Tan,
353 Ramin Mohammad Hosseini Dokht, Wen-che Yu, Lingsen Meng, Hui Huang, Jean Schmittbuhl,
354 Marco Bohnhoff, Christopher Wollin, Tomoaki Nishikawa, Emily Warren-Smith, Luis A.
355 Dominguez, Tianhaozhe Sun, and Haipeng Luo are much appreciated. The HRSN and Fox Creek

356 event waveform data used in this study were downloaded from the Northern California
 357 Earthquake Data Center (NCEDC) (<http://ncedc.org/hrsn/>) and Incorporated Research
 358 Institutions for Seismology (IRIS) (<http://ds.iris.edu/ds/nodes/dmc/>), respectively. Seismic data
 359 are processed with Obspy (*Beyreuther et al.*, 2010; <https://github.com/obspy/obspy/>). Figures are
 360 made with Matplotlib (*Hunter*, 2007; <https://matplotlib.org>) and Inkscape (<https://inkscape.org>).
 361 This study is partially supported by a University of Victoria Fellowship (DG), the Induced
 362 Seismicity Research Project of NRCAN (HK), Geoscience BC (HK), and a NSERC Discovery
 363 Grant (HK). This paper is NRCAN contribution 2021xxxx.

364
 365

366 **References**

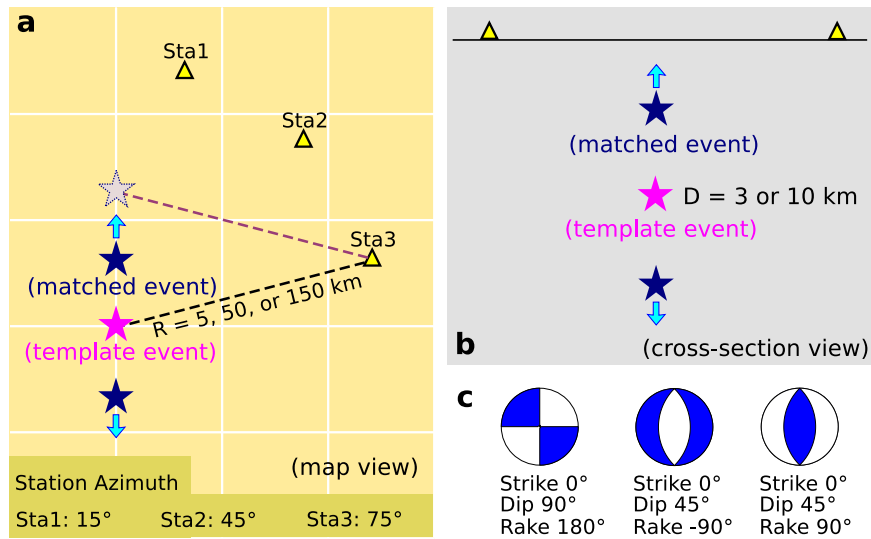
- 367 Abercrombie, R. E. (2014). Stress drops of repeating earthquakes on the San Andreas fault at
 368 Parkfield. *Geophysical Research Letters*, *41*(24), 8784-8791.
- 369 Beyreuther, M., Barsch, R., Krischer, L., Megies, T., Behr, Y., & Wassermann, J. (2010). ObsPy:
 370 A Python toolbox for seismology. *Seismological Research Letters*, *81*(3), 530-533.
- 371 Bohnhoff, M., Wollin, C., Domigall, D., Küperkoch, L., Martínez-Garzón, P., Kwiatek, G., ... &
 372 Malin, P. E. (2017). Repeating Marmara Sea earthquakes: indication for fault
 373 creep. *Geophysical Journal International*, *210*(1), 332-339.
- 374 Bouchon, M., Karabulut, H., Aktar, M., Özalaybey, S., Schmittbuhl, J., & Bouin, M. P. (2011).
 375 Extended nucleation of the 1999 Mw 7.6 Izmit earthquake. *science*, *331*(6019), 877-880.
- 376 Brune, J. N. (1970). Tectonic stress and the spectra of seismic shear waves from
 377 earthquakes. *Journal of geophysical research*, *75*(26), 4997-5009.
- 378 Chamberlain, C. J., & Townend, J. (2018). Detecting Real Earthquakes Using Artificial
 379 Earthquakes: On the Use of Synthetic Waveforms in Matched-Filter Earthquake
 380 Detection. *Geophysical Research Letters*, *45*(21), 11-641.
- 381 Chamberlain, C. J., Hopp, C. J., Boese, C. M., Warren-Smith, E., Chambers, D., Chu, S. X., ... &
 382 Townend, J. (2018). EQcorrscan: Repeating and near-repeating earthquake detection and
 383 analysis in python. *Seismological Research Letters*, *89*(1), 173-181.
- 384 Cheng, X., Niu, F., Silver, P. G., Horiuchi, S., Takai, K., Iio, Y., & Ito, H. (2007). Similar
 385 microearthquakes observed in western Nagano, Japan, and implications for rupture
 386 mechanics. *Journal of Geophysical Research: Solid Earth*, *112*(B4).
- 387 Ellsworth, W. L., & Bulut, F. (2018). Nucleation of the 1999 Izmit earthquake by a triggered
 388 cascade of foreshocks. *Nature Geoscience*, *11*(7), 531-535.
- 389 Gao, D., & Kao, H. (2020). Optimization of the Match-Filtering Method for Robust Repeating
 390 Earthquake Detection: The Multisegment Cross-Correlation Approach. *Journal of*
 391 *Geophysical Research: Solid Earth*, *125*(7), e2020JB019714.
- 392 Hayward, T. W., & Bostock, M. G. (2017). Slip behavior of the queen Charlotte plate boundary
 393 before and after the 2012, MW 7.8 Haida Gwaii earthquake: evidence from repeating
 394 earthquakes. *Journal of Geophysical Research: Solid Earth*, *122*(11), 8990-9011.

- 395 Hotovec-Ellis, A. J., & Jeffries, C. (2016). Near real-time detection, clustering, and analysis of
 396 repeating earthquakes: Application to Mount St. Helens and Redoubt volcanoes.
 397 In *Seismological Society of America Annual Meeting*.
- 398 Huang, H., & Meng, L. (2018). Slow unlocking processes preceding the 2015 Mw 8.4 Illapel,
 399 Chile, earthquake. *Geophysical Research Letters*, *45*(9), 3914-3922.
- 400 Hunter, J. D. (2007). Matplotlib: A 2D graphics environment. *IEEE Annals of the History of*
 401 *Computing*, *9*(03), 90-95.
- 402 Jiang, C., Wu, Z., Li, Y., & Ma, T. (2014). “Repeating Events” as Estimator of Location
 403 Precision: The China National Seismograph Network. *Pure and Applied Geophysics*, *171*(3-
 404 5), 413-423.
- 405 Kato, A., & Nakagawa, S. (2014). Multiple slow-slip events during a foreshock sequence of the
 406 2014 Iquique, Chile Mw 8.1 earthquake. *Geophysical Research Letters*, *41*(15), 5420-5427.
- 407 Kato, A., Obara, K., Igarashi, T., Tsuruoka, H., Nakagawa, S., & Hirata, N. (2012). Propagation
 408 of slow slip leading up to the 2011 Mw 9.0 Tohoku-Oki earthquake. *Science*, *335*(6069), 705-
 409 708.
- 410 Li, A., & Richards, P. G. (2003). Using earthquake doublets to study inner core rotation and
 411 seismicity catalog precision. *Geochemistry, Geophysics, Geosystems*, *4*(9).
- 412 Li, L., Chen, Q. F., Cheng, X., & Niu, F. (2007). Spatial clustering and repeating of seismic
 413 events observed along the 1976 Tangshan fault, north China. *Geophysical research*
 414 *letters*, *34*(23).
- 415 Li, L., Chen, Q. F., Niu, F., & Su, J. (2011). Deep slip rates along the Longmen Shan fault zone
 416 estimated from repeating microearthquakes. *Journal of Geophysical Research: Solid*
 417 *Earth*, *116*(B9).
- 418 Materna, K., Taira, T. A., & Bürgmann, R. (2018). Aseismic transform fault slip at the
 419 Mendocino triple junction from characteristically repeating earthquakes. *Geophysical*
 420 *Research Letters*, *45*(2), 699-707.
- 421 Matsubara, M., Yagi, Y., & Obara, K. (2005). Plate boundary slip associated with the 2003 Off-
 422 Tokachi earthquake based on small repeating earthquake data. *Geophysical Research*
 423 *Letters*, *32*(8).
- 424 Meier, T., Rische, M., Endrun, B., Vafidis, A., & Harjes, H. P. (2004). Seismicity of the Hellenic
 425 subduction zone in the area of western and central Crete observed by temporary local seismic
 426 networks. *Tectonophysics*, *383*(3-4), 149-169.
- 427 Meng, L., Huang, H., Bürgmann, R., Ampuero, J. P., & Strader, A. (2015). Dual megathrust slip
 428 behaviors of the 2014 Iquique earthquake sequence. *Earth and Planetary Science*
 429 *Letters*, *411*, 177-187.
- 430 Nadeau, R. M., & Johnson, L. R. (1998). Seismological studies at Parkfield VI: Moment release
 431 rates and estimates of source parameters for small repeating earthquakes. *Bulletin of the*
 432 *Seismological Society of America*, *88*(3), 790-814.

- 433 Pacheco, K., Nishimura, T., & Nakahara, H. (2017). Seismic velocity changes of P and S waves
 434 associated with the 2011 Tohoku-Oki earthquake (M w 9.0) as inferred from analyses of
 435 repeating earthquakes. *Geophysical Journal International*, 209(1), 517-533.
- 436 Poupinet, G., Ellsworth, W. L., & Frechet, J. (1984). Monitoring velocity variations in the crust
 437 using earthquake doublets: An application to the Calaveras Fault, California. *Journal of*
 438 *Geophysical Research: Solid Earth*, 89(B7), 5719-5731.
- 439 Sáez, M., Ruiz, S., Ide, S., & Sugioka, H. (2019). Shallow nonvolcanic tremor activity and
 440 potential repeating earthquakes in the Chile Triple Junction: seismic evidence of the
 441 subduction of the active Nazca–Antarctic spreading center. *Seismological Research*
 442 *Letters*, 90(5), 1740-1747.
- 443 Sawazaki, K., Kimura, H., Shiomi, K., Uchida, N., Takagi, R., & Snieder, R. (2015). Depth-
 444 dependence of seismic velocity change associated with the 2011 Tohoku earthquake, Japan,
 445 revealed from repeating earthquake analysis and finite-difference wave propagation
 446 simulation. *Geophysical Journal International*, 201(2), 741-763.
- 447 Schaff, D. P., & Beroza, G. C. (2004). Coseismic and postseismic velocity changes measured by
 448 repeating earthquakes. *Journal of Geophysical Research: Solid Earth*, 109(B10).
- 449 Schaff, D. P., & Richards, P. G. (2011). On finding and using repeating seismic events in and
 450 near China. *Journal of Geophysical Research: Solid Earth*, 116(B3).
- 451 Stein, S., & Wysession, M. (2009). *An introduction to seismology, earthquakes, and earth*
 452 *structure*. John Wiley & Sons.
- 453 Tepp, G. (2018). A repeating event sequence alarm for monitoring volcanoes. *Seismological*
 454 *Research Letters*, 89(5), 1863-1876.
- 455 Tkalčić, H., Young, M., Bodin, T., Ngo, S., & Sambridge, M. (2013). The shuffling rotation of
 456 the Earth's inner core revealed by earthquake doublets. *Nature Geoscience*, 6(6), 497-502.
- 457 Uchida, N. (2019). Detection of repeating earthquakes and their application in characterizing
 458 slow fault slip. *Progress in Earth and Planetary Science*, 6(1), 40.
- 459 Uchida, N., & Bürgmann, R. (2019). Repeating earthquakes. *Annual Review of Earth and*
 460 *Planetary Sciences*, 47, 305-332.
- 461 Uchida, N., Matsuzawa, T., Hasegawa, A., & Igarashi, T. (2003). Interplate quasi-static slip off
 462 Sanriku, NE Japan, estimated from repeating earthquakes. *Geophysical Research*
 463 *Letters*, 30(15).
- 464 Uchida, N., Matsuzawa, T., Hirahara, S., & Hasegawa, A. (2006). Small repeating earthquakes
 465 and interplate creep around the 2005 Miyagi-oki earthquake (M= 7.2). *Earth, planets and*
 466 *space*, 58(12), 1577-1580.
- 467 Waldhauser, F., & Ellsworth, W. L. (2000). A double-difference earthquake location algorithm:
 468 Method and application to the northern Hayward fault, California. *Bulletin of the*
 469 *Seismological Society of America*, 90(6), 1353-1368.
- 470 Wang, B., Harrington, R. M., Liu, Y., Kao, H., & Yu, H. (2020). A study on the largest
 471 hydraulic-fracturing-induced earthquake in Canada: Observations and static stress-drop
 472 estimation. *Bulletin of the Seismological Society of America*, 110(5), 2283-2294.

- 473 Wu, W., Zhan, Z., Peng, S., Ni, S., & Callies, J. (2020). Seismic ocean
474 thermometry. *Science*, 369(6510), 1510-1515.
- 475 Yamada, M., Mori, J., & Matsushi, Y. (2016). Possible stick-slip behavior before the Rausu
476 landslide inferred from repeating seismic events. *Geophysical Research Letters*, 43(17), 9038-
477 9044.
- 478 Yao, D., Walter, J. I., Meng, X., Hobbs, T. E., Peng, Z., Newman, A. V., ... & Protti, M. (2017).
479 Detailed spatiotemporal evolution of microseismicity and repeating earthquakes following the
480 2012 Mw 7.6 Nicoya earthquake. *Journal of Geophysical Research: Solid Earth*, 122(1), 524-
481 542.
- 482 Yu, W. C. (2013). Shallow-focus repeating earthquakes in the Tonga–Kermadec–Vanuatu
483 subduction zones. *Bulletin of the Seismological Society of America*, 103(1), 463-486.
- 484 Zhang, J., Richards, P. G., & Schaff, D. P. (2008). Wide-scale detection of earthquake waveform
485 doublets and further evidence for inner core super-rotation. *Geophysical Journal
486 International*, 174(3), 993-1006.
- 487 Zhang, J., Song, X., Li, Y., Richards, P. G., Sun, X., & Waldhauser, F. (2005). Inner core
488 differential motion confirmed by earthquake waveform doublets. *Science*, 309(5739), 1357-
489 1360.
490

491



492

493

Figure 1. Schematic diagram showing the setup of the synthetic experiments. (a) For horizontal

inter-event separation, two sources are placed along a line trending N–S separated by a short

distance. The template event (fuchsia star) is fixed in the middle while the matched event (navy

blue star) moves away from the template event in both directions. Stations (triangles) are placed

at three different epicentral distances ($R=5, 50, \text{ or } 150 \text{ km}$). The gray star marks the location of

the matched event such that one of the stations (Sta3 in this case) is of equal distance to both the

template and matched events. (b) For vertical inter-event separation, the template event is placed

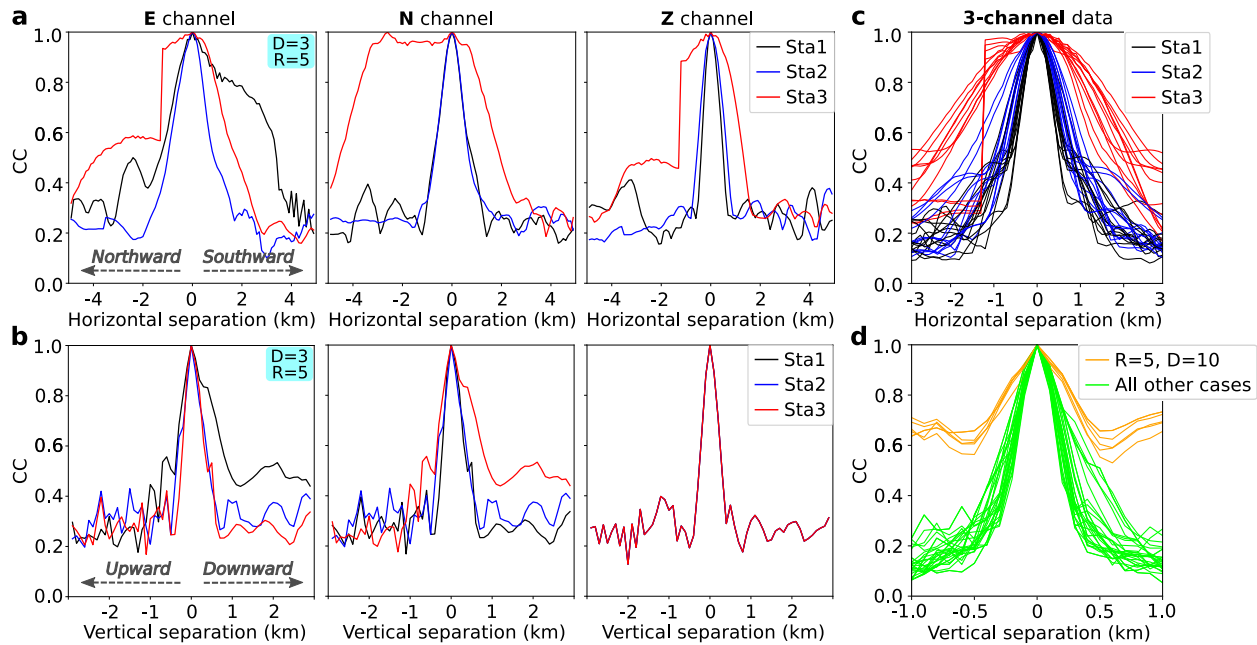
at two different depths ($D=3 \text{ or } 10 \text{ km}$) with the matched event moving up or down. (c) Three

different types of focal mechanisms are used in the calculation of synthetic seismograms.

502

503

504



505

506

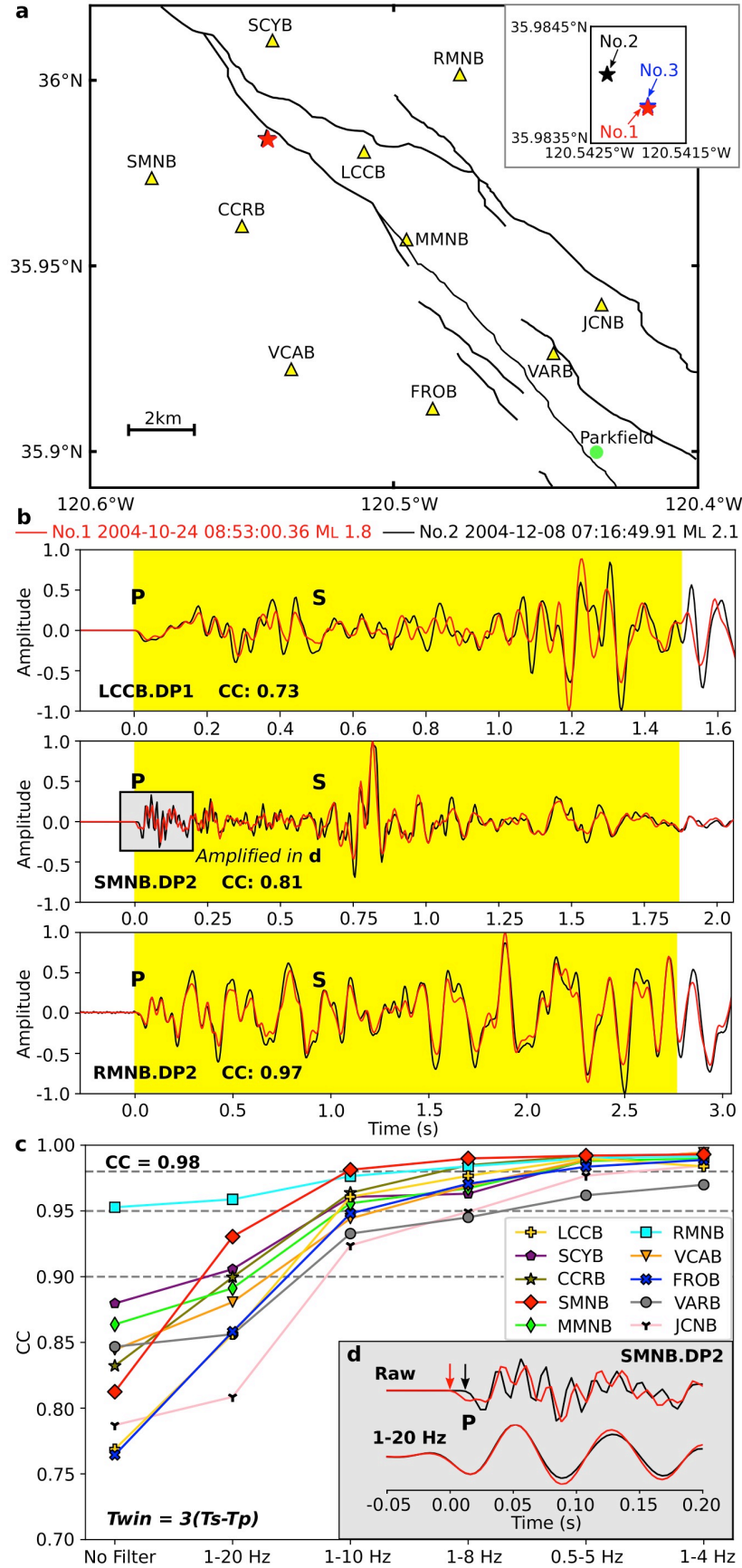
Figure 2. Results of our synthetic experiment showing CC variation as a function of horizontal (a and c) and vertical (b and d) inter-event separation. The setup of sources and receivers is depicted in Figure 1. (a) and (b) correspond to a representative case with single-channel data, whereas (c) and (d) compile all test results with single-station (3-channel) data. Individual test results are presented in Figures S3 and S4. For (a) and (c), positive and negative values along the X axis mean that the matched event is shifted to the south and north, respectively; for (b) and (d), positive and negative X axis mean that the matched event moves downward and upward, respectively.

513

514

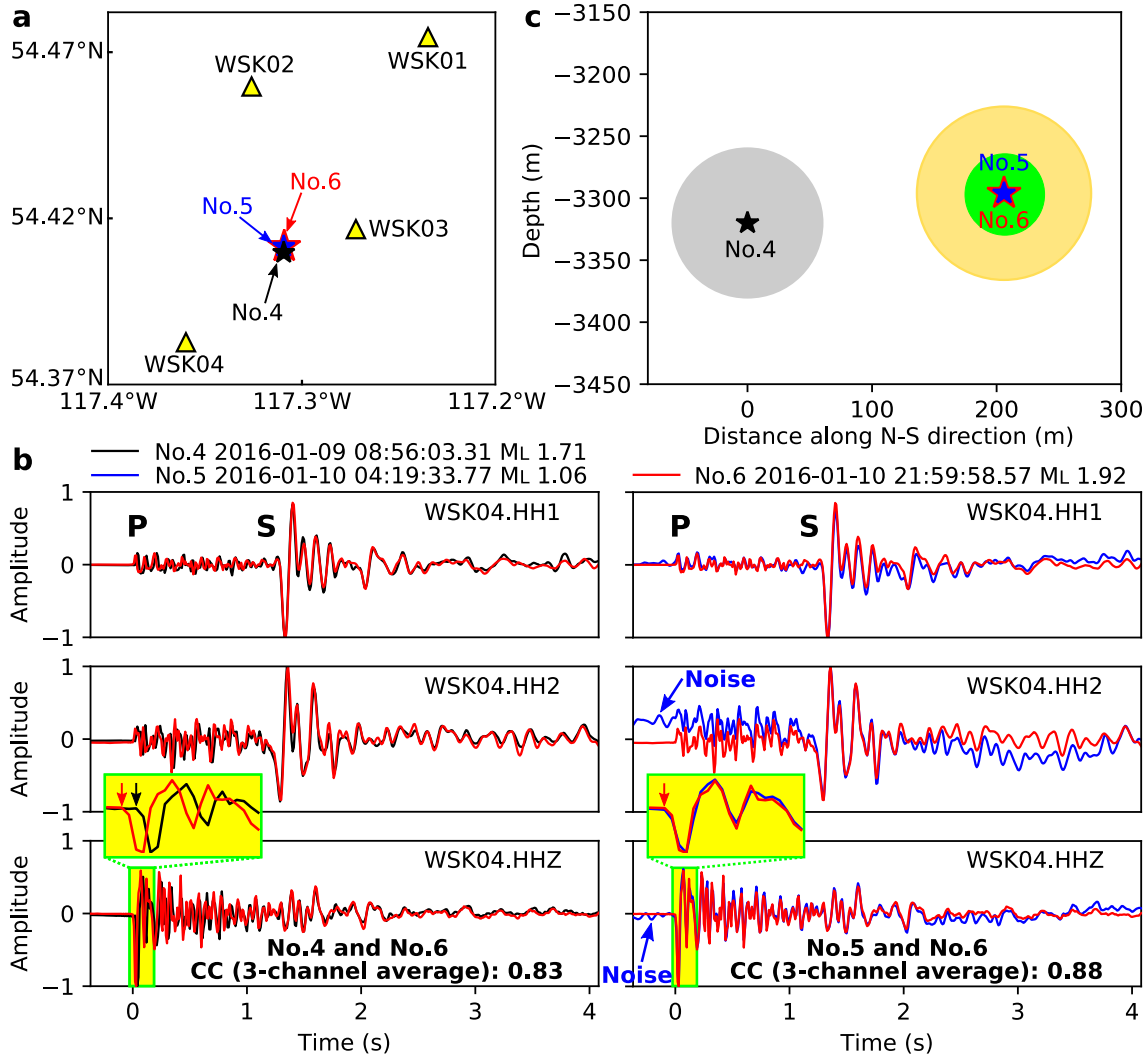
515

516



518 **Figure 3.** CC test results with real earthquake data. (a) Map showing the distribution of
519 earthquake epicenters (colored stars) and HRSN seismograph stations (yellow triangles). Black
520 lines denote the surface traces of the San Andreas Fault system. The town of Parkfield is shown
521 as a green dot. Insert shows the zoom-in locations of events No. 1-3. (b) Examples of normalized
522 unfiltered waveforms of two events that have been verified to be non-repeaters (No. 1 and No.
523 2), aligned at the S wave arrival. The highlighted segment indicates the window of dynamic
524 length (see Text S2) used for CC calculation. The gray box in the middle panel outlines the
525 waveform segment amplified in (d). (c) Effects of filtering on the CC values between events No.
526 1 and No. 2 determined with individual single-station (3-channel) data and dynamic window
527 lengths. (d) An example of waveform change due to filtering. Red and black arrows mark the P
528 wave onset of events No.1 and No.2, respectively. The slight time difference (0.012 s) between
529 the two arrows is overlooked after band-pass filtering between 1 and 20 Hz.
530
531
532

533
534



535
536 **Figure 4.** A physics-based approach to distinguish repeating and neighboring events. (a) Map
537 showing the distribution of earthquake epicenters (colored stars) and seismograph stations
538 (yellow triangles). A zoom-in map of the source area is presented in Figure S11. (b) Normalized
539 unfiltered waveforms, aligned at the S wave arrival. Notice the apparent time difference in the S-
540 P differential traveltime between the two cases. (c) North-south cross section showing the
541 relative event locations. Gray, lime, and gold circles are the ERRs of events No. 4, 5 and 6,
542 respectively. The stress drops of events No. 4 and 6 are 35 and 30 MPa, respectively, based on
543 the spectral ratio analysis of the broadband waveforms (*Wang et al.*, 2020). Since the waveforms
544 of event No. 5 is contaminated by a high level of noise, its stress drop is assumed to be the
545 average of events No. 4 and 6 (i.e., 32.5 MPa).

Identification of Repeating Earthquakes:

Misconception of Waveform Similarity and a Physics-based Solution

Dawei Gao^{1,2} and Honn Kao^{1,2}

¹School of Earth and Ocean Sciences, University of Victoria, Victoria, British Columbia, Canada

²Pacific Geoscience Centre, Geological Survey of Canada, Sidney, British Columbia, Canada

Contents of this file

Texts S1–S3
Figures S1–S11
Tables S1–S3

Introduction

This Supporting Information provides additional texts, figures, and tables to further strengthen the arguments and findings presented in the main text. Texts S1, S2 and S3 describes the technical details of the synthetic experiment setup, the CC calculation, and the DTDD method, respectively. Figure S1 shows an example of synthetic waveforms of both template and matched events for an assumed strike-slip focal mechanism. Figure S2 demonstrates the CC variation as a function of inter-event separation using single-channel waveform data for a normal-faulting focal mechanism. Figures S3 and S4 summarize the testing results of CC variation (obtained with single-station, 3-channel data) due to horizontal and vertical inter-event separations, respectively. Figure S5 illustrates the effects of filtering on CC between non-repeaters (events No. 1 and No. 2) with single-channel data at each station. Figure S6 displays the results of using different window lengths and band-pass filters in determining CC between non-repeaters with single-station (3-channel) data. Figures S7 and S8 illustrate how different band-pass filters could affect waveform similarity at close and distant stations, respectively. Figure S9 demonstrates the effects of window length and filtering in calculating CC between true repeaters (events No. 1 and No. 3). Figure S10 shows the examples of normalized unfiltered waveforms of true repeaters (No. 1 and 3). Figure S11 provides the zoom-in

location map of the Fox Creek events (No. 4-6). Table S1 is a compiled list of different criteria in identifying repeaters. Tables S2 and S3 summarize the commonly used digital filters and commonly assumed stress drop values in previous studies, respectively.

Text S1. Synthetic Experiment Setup

The configuration of our synthetic experiments is shown in Figure 1. Due to the symmetrical setup of our experiment, it is sufficient to focus our investigation on stations in the first quadrant. For the demonstration purpose, we place three stations at the azimuths of 15° , 45° , and 75° , respectively. To explore the effects from various source parameters, we conduct our tests with two different focal depths ($D = 3$ or 10 km), three representative focal mechanisms (strike-slip, normal, or reverse faulting), and three different epicentral distances ($R = 5, 50, \text{ or } 150$ km, Figure 1). In total, 36 scenarios that correspond to either horizontal (± 5 km) or vertical (± 3 km) inter-event separation are studied in detail. The synthetic seismograms are generated and processed exactly the same way as an earlier study (Gao and Kao, 2020). The details of CC calculation are presented in Text S2.

Text S2. CC Calculation

To calculate the CC value of an earthquake pair, we utilize the recently developed match-filtering with multi-segment cross-correlation (MFMC) technique (Gao and Kao, 2020) instead of the classical cross-correlation method which can be severely biased by the existence of large-amplitude phases such as S wave and surface waves (e.g., Kraft and Deichmann, 2014; Myhill et al., 2011; Li et al., 2017; Gao and Kao, 2020). Compared with the conventional one-segment approach, the MFMC technique splits the template into a number of consecutive segments during the cross-correlation process. Such a procedure is designed to mitigate the impact of the large-amplitude phases and essentially gives more weights to important low-amplitude phases such as depth phases (Ma and Atkinson, 2006; Ma, 2010) and coda waves (Snieder and Vrijlandt, 2005; Robinson et al., 2011) that carry additional source location information. Thus the MFMC technique is more reliably in capturing the waveform discrepancy and differentiating the source location difference between an event pair (Gao and Kao, 2020).

In our MFMC CC calculation, we first cut the waveform from the template event starting at the onset of the P wave with a length of T_{win} . For synthetic experiments, we use a dynamic template window length of $T_{\text{win}} = 3(T_s - T_p)$, where T_s and T_p are the S- and P-phase arrival times, respectively. Using a dynamic template window length based on the differential traveltimes between P and S phases is necessary to properly account for the increasing wave train with epicentral distance ($R = 5, 50, \text{ or } 150$ km in our experiment, Figure 1a) (Baisch et al., 2008; Gao and Kao, 2020). For real earthquake waveform tests in Parkfield area, we tested both dynamic (i.e., $3(T_s - T_p)$) and fixed T_{win} (1.5 s, 3.0 s, 4.5 s, and 6.0 s) for each station given the small study area (Figure 3a). It should be noted that a fixed T_{win} of 6.0 s, equivalent to $12(T_s - T_p)$ of the closest station LCCB (Figure 3a), is sufficiently long covering much of the low-amplitude coda waves. Then the template waveform is divided into N_{seg} segments of equal length. For

unfiltered waveforms, N_{seg} is assigned as 4; for filtered waveforms, the value of N_{seg} is determined by the cycles of the longest period wave ($1/f_{\text{min}}$) in the band-pass filtered waveform (i.e., $N_{\text{seg}} = T_{\text{win}} \times f_{\text{min}}$) and the minimum value of N_{seg} is set to be 4 as suggested by an earlier study (Gao and Kao, 2020). At last, all the segments are shifted together one sample point at a time from 0.5 s before the P arrival of the targeted event to 0.5 s after. The cross-correlation calculation is performed individually for each segment, and the CC value at each sample point is given by the average of all segments. The maximum CC value of all time steps is defined as the final CC value of the earthquake pair. If data from three channels of the same station are used, the CC value of all time steps from all three channels are averaged, and the maximum within the sliding window is taken as the final CC.

Text S3. The Differential Traveltime Double-Difference (DTDD) Method

To precisely estimate the relative location between an event pair, we develop the differential traveltime double-difference (DTDD) method which minimizes the residual between observed and predicted relative S-P differential traveltime through three-dimensional (3D) grid search. The relative S-P differential traveltime, ΔSP_{ij}^k , between events i and j at station k is given by:

$$\Delta SP_{ij}^k = SP_i^k - SP_j^k \quad (1)$$

where SP_i^k and SP_j^k are the S-P differential traveltimes of events i and j at station k , respectively. If we take the event i as the reference, the relative location of event j is obtained by searching all the possible locations around the reference event in a 3D space. The best location is defined as the grid node which yields the minimum sum of the residuals, R , between observed and predicted relative S-P differential traveltimes:

$$R = \sum_k |(\Delta SP_{ij}^k)^{\text{obs}} - (\Delta SP_{ij}^k)^{\text{cal}}| \quad (2)$$

where $(\Delta SP_{ij}^k)^{\text{obs}}$ and $(\Delta SP_{ij}^k)^{\text{cal}}$ are the observed and theoretical relative S-P differential traveltimes, respectively. Combining (1) and (2) yields:

$$R = \sum_k |(SP_i^k - SP_j^k)^{\text{obs}} - (SP_i^k - SP_j^k)^{\text{cal}}| \quad (3)$$

which is the double-difference of the S-P differential traveltime. It should be noted that, in the measure of misfit (Equations 2 and 3), we use the L1 normal instead of the widely used L2 norm (least squares) because L1 normal is more robust and less sensitive to outliers (Shearer, 1997; Shearer, 2009; Trugman and Shearer, 2017).

When implementing the 3D grid search, we employ a two-step strategy to minimize the calculation, i.e., using a large grid size for initial locating and a very small one for the final solution. Taking the Fox Creek events (No. 4-6) for example, we take the largest event No. 6 as the reference location and define the search volume as the cubic space of 1 km \times 1 km \times 1 km centred at the reference event. The preliminary solution is determined with a grid search at the spacing of 10 m. Once the preliminary location is identified, we conduct a finer search at the interval of 1 m within the 20 m \times 20 m \times 20 m cubic space centred at the preliminary solution to obtain the final solution. The effectiveness of our

approach is evident from the located results shown in Figure S11. The hypocentres of both reference (No. 6) and located (No. 4 and No. 5) events generally fall on a line trending N-S, consistent with the inference of a local N-S trending strike-slip fault system (Schultz et al., 2017; Wang et al., 2017).

Compared with the conventional grid search approach which scans all possible locations and origin times to minimize the time residuals between observed and theoretical traveltimes of certain phases (e.g., P and/or S phases; Shearer, 2009), one obvious advantage of the DTDD method is that the relative position is determined without the events' origin times. This formulation effectively avoids the trade-off problem between origin time and source depth. Another added benefit is that it can cancel any path effects due to unmodeled velocity heterogeneities. We note that precise relative location based on the relative S-P differential traveltime can also be solved by conventional inversion schemes (e.g., Cheng et al., 2007). However, the conventional inversion approach may suffer from being trapped to local minima, whereas the forward grid-search approach adopted by the DTDD method always find the global minimum.

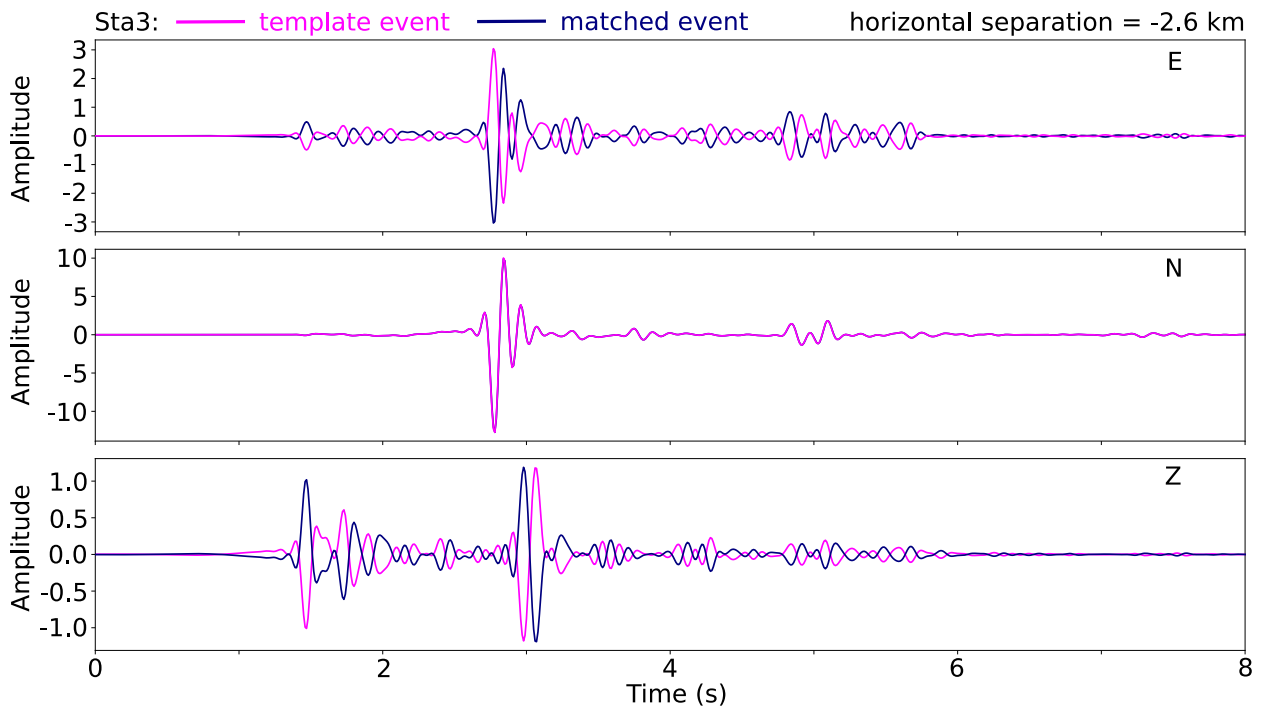


Figure S1. Synthetic waveforms of both template and matched events for a horizontal separation of -2.6 km. The template event is a strike-slip earthquake and is placed at the depth of 3 km. The receiver has an epicentral distance of 5 km with respect to the template event.

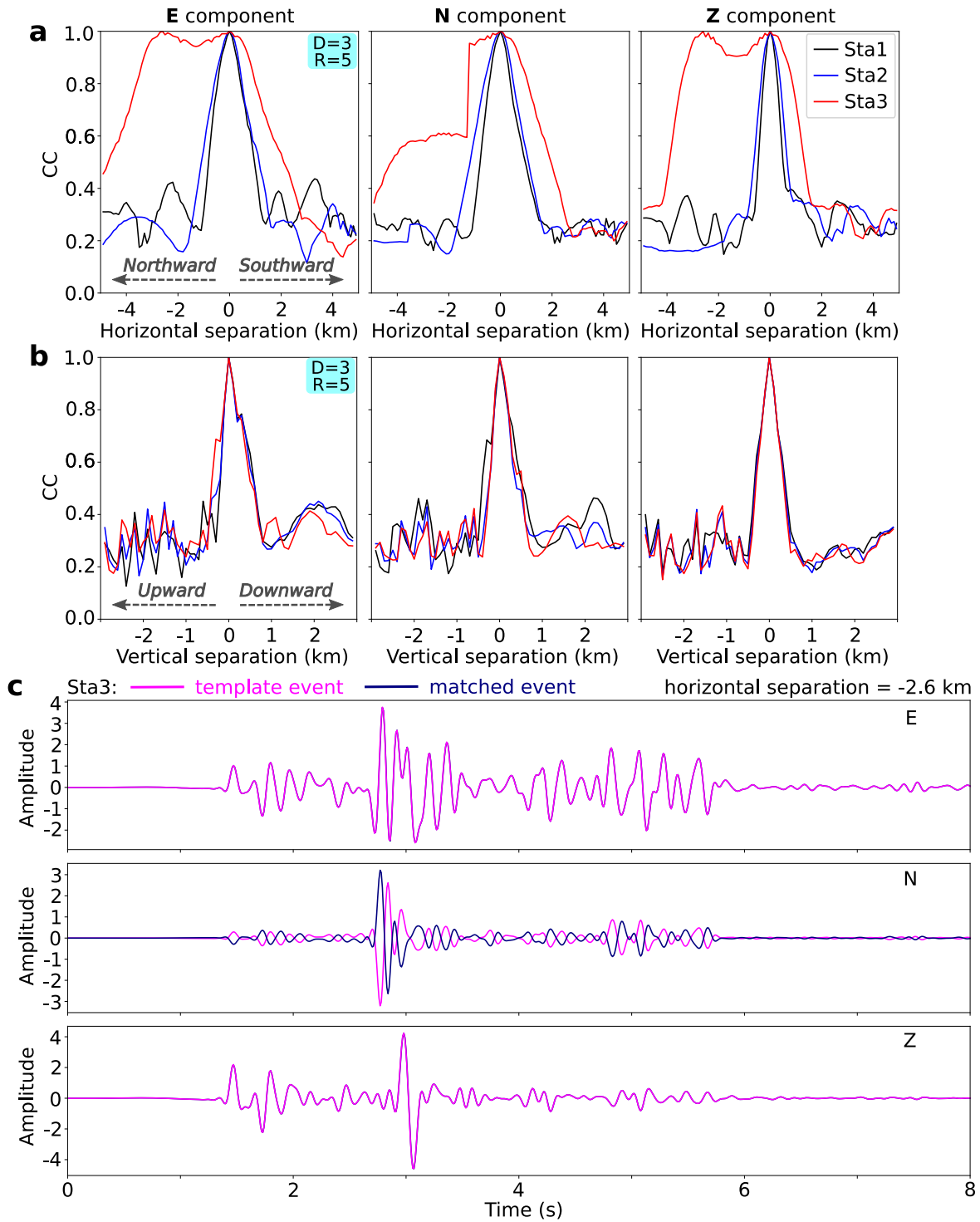


Figure S2. CC variation (obtained with single-channel data) due to inter-event separations. The template event is a normal-faulting earthquake at the depth of 3 km. The receiver has an epicentral distance of 5 km with respect to the template event. (a) CC variation due to horizontal separations. (b) CC variation due to vertical separations. (c) Synthetic waveforms of both template and matched events for a horizontal separation of -2.6 km.

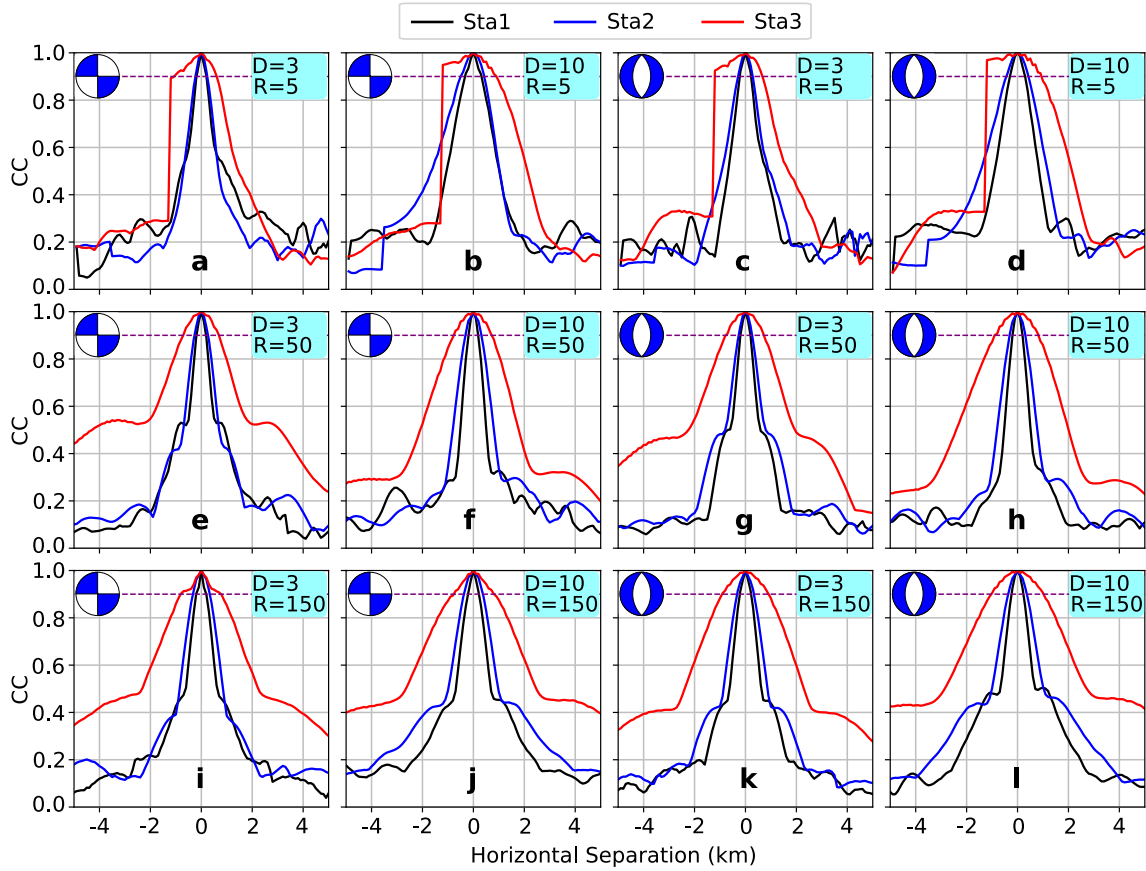


Figure S3. CC variation (obtained with single-station, 3-channel data) due to horizontal inter-event separations. Dashed purple line marks the CC value of 0.90 for reference. Note that the results of a reverse fault are the same as those of a normal fault and hence are not displayed.

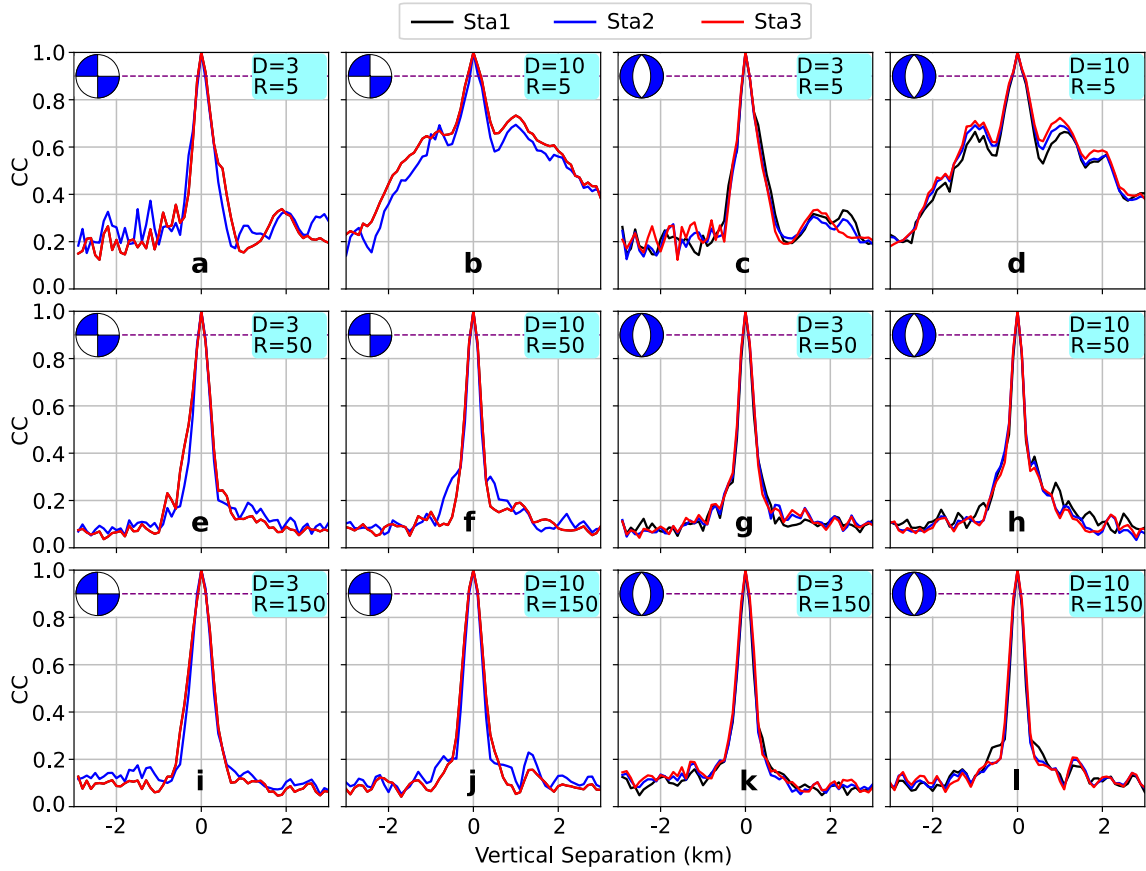


Figure S4. CC variation (obtained with single-station, 3-channel data) due to vertical inter-event separations. Layout is the same as Figure S3. Note that the results of a reverse fault are the same as those of a normal fault and hence are not displayed.

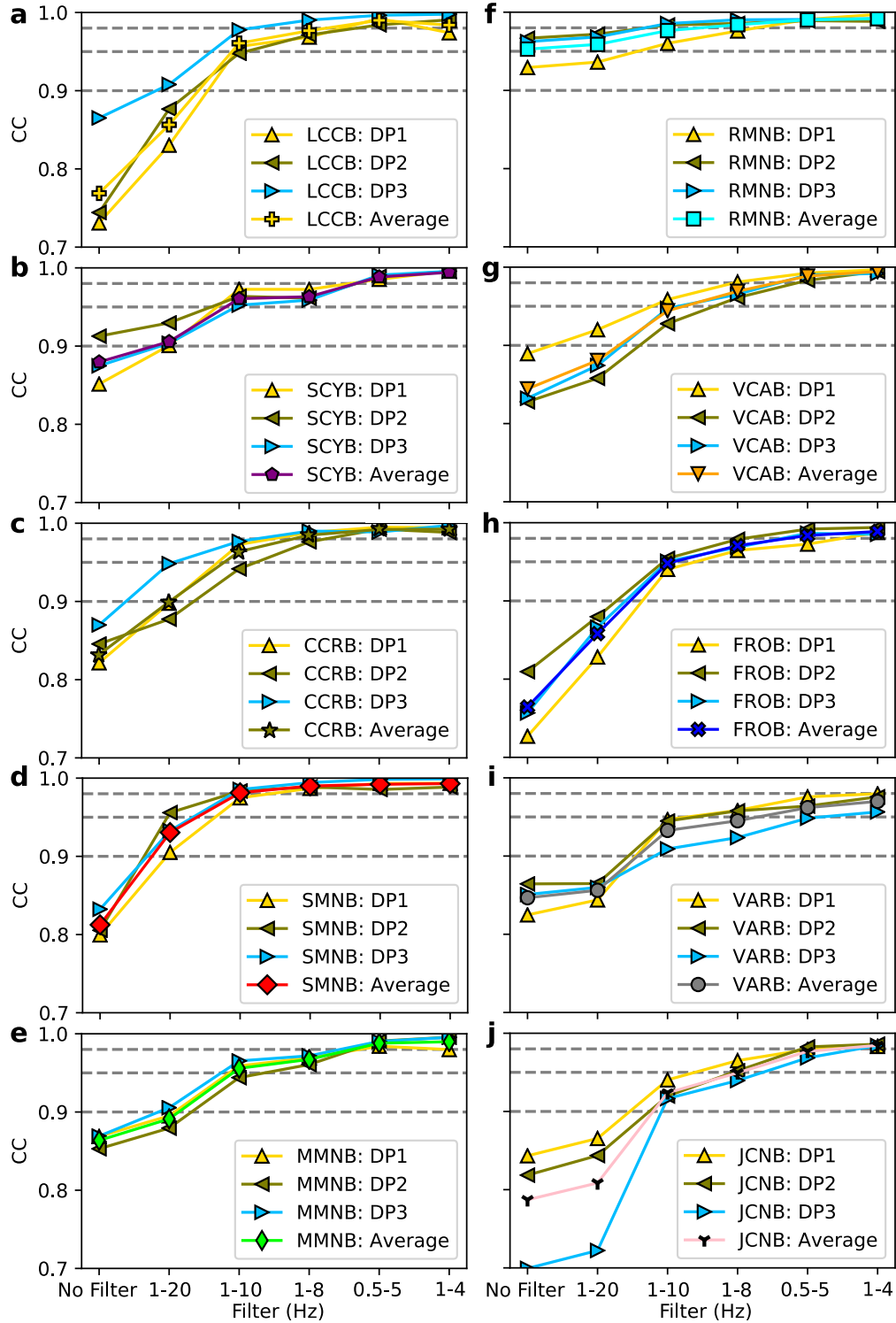


Figure S5. Effects of filtering on the CC value between two events that have been verified to be non-repeaters (events No. 1 and No. 2, Figure 3) with single-channel data. All CC values are determined with the dynamic T_{win} (see Text S2 for more details). For each panel, the station and channel names (e.g., LCCB: DP1) are given in the legend box.

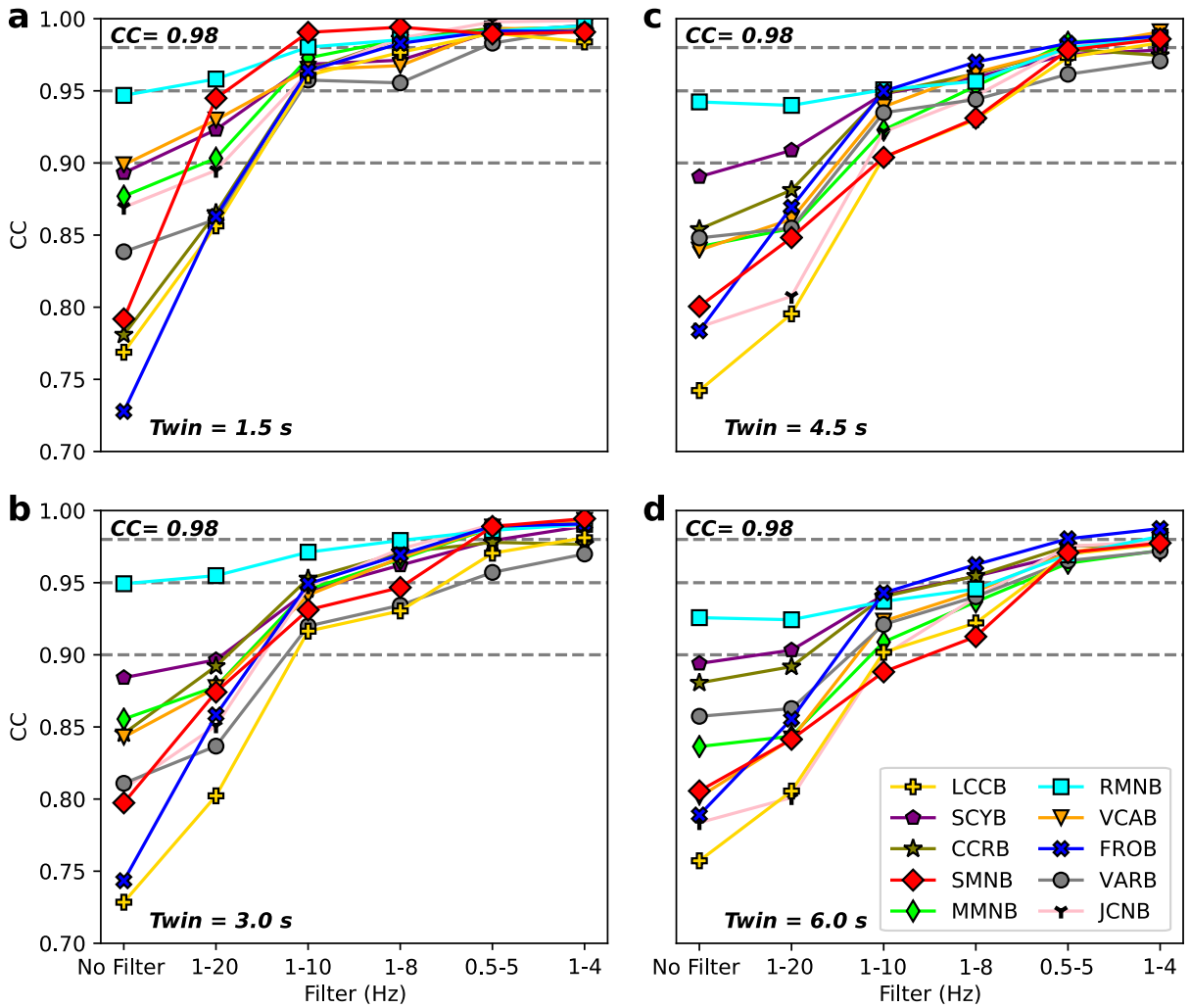


Figure S6. Effects of T_{win} and filtering on the CC value between two events that have been verified to be non-repeaters (events No. 1 and No. 2, Figure 3) with single-station (3-channel) data. (a)-(d) correspond to the T_{win} of 1.5, 3.0, 4.5 and 6.0 s, respectively.

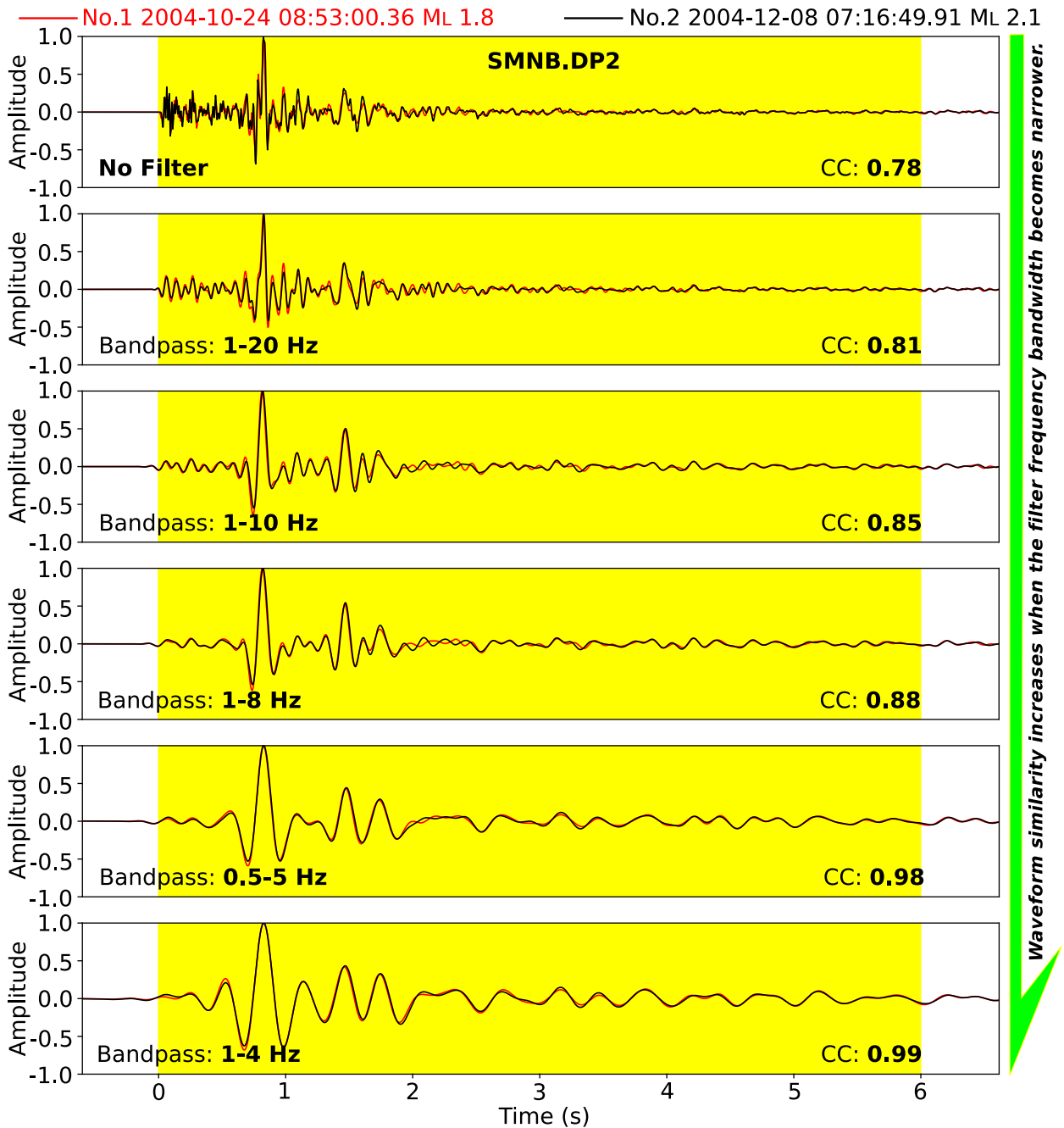


Figure S7. An example of how filtering increases waveform similarity at a close station SMNB. The highlighted segment ($T_{win} = 6.0$ s) is used to calculate the CC value which is labelled at the lower-right corner. Note that a T_{win} of 6.0 s, equivalent to $10(T_s - T_p)$ at station SMNB, is sufficiently long to cover much of the low-amplitude coda waves.

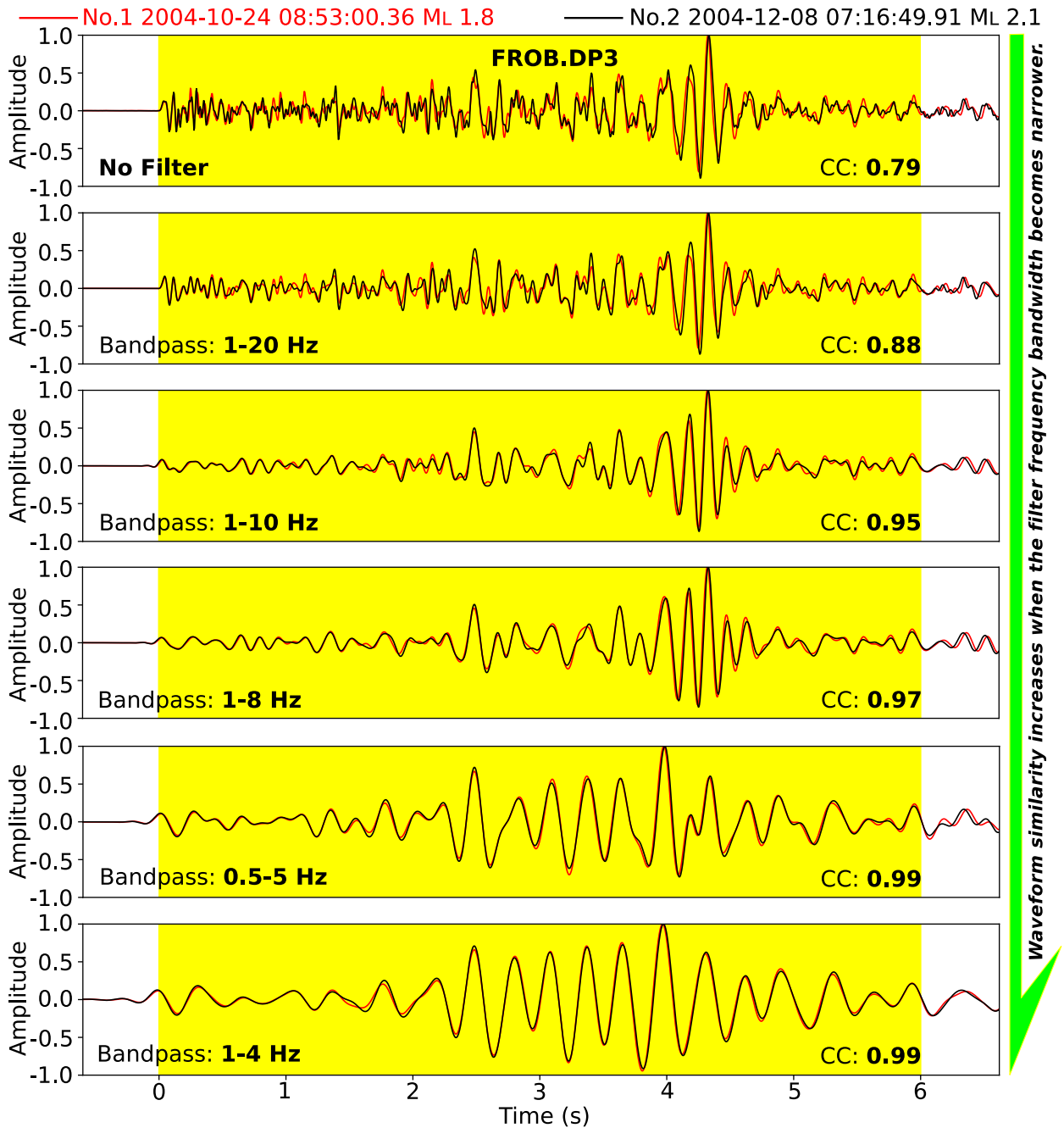


Figure S8. An example of how filtering increases waveform similarity at a distant station FROB. Layout is the same as Figure S7.

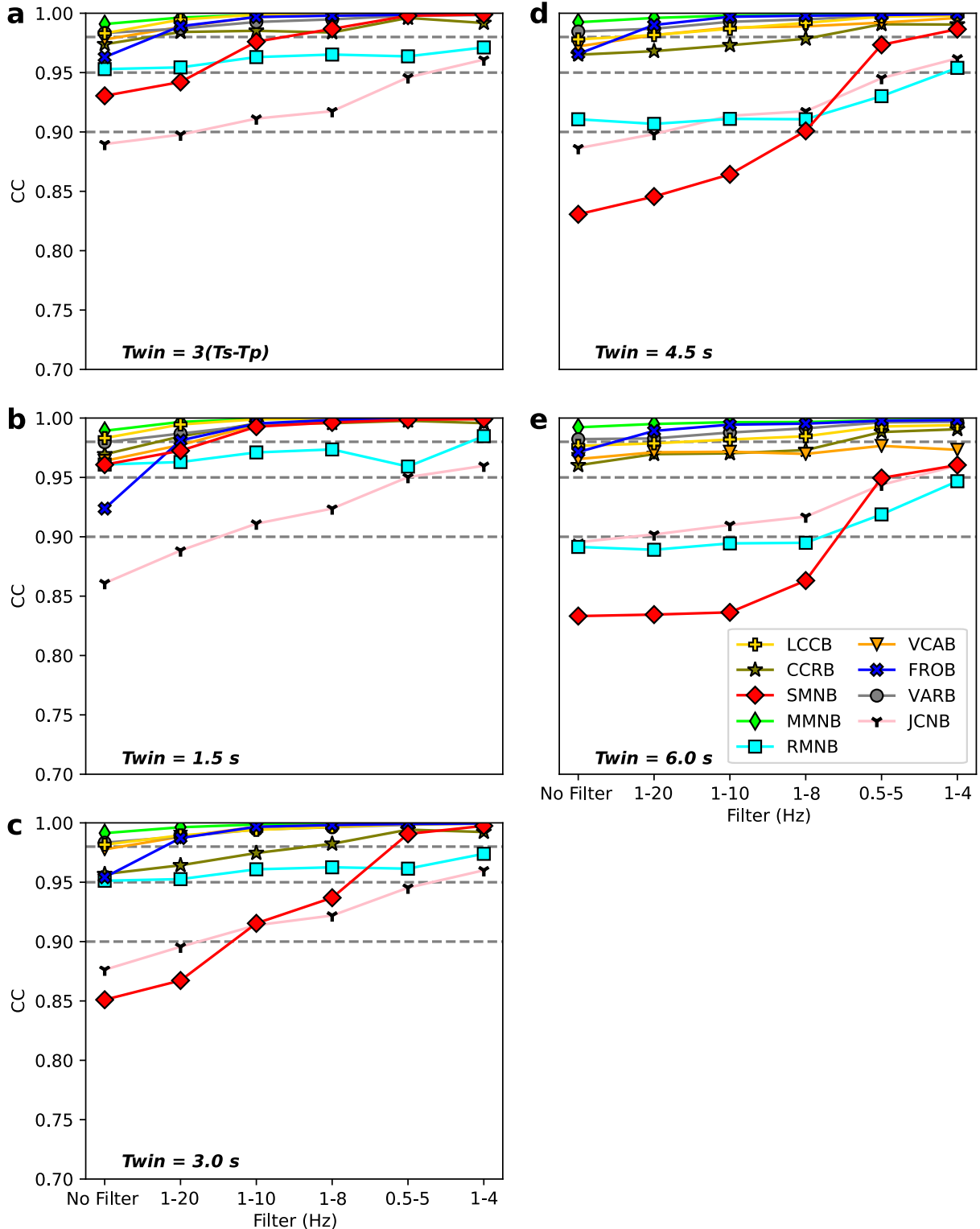


Figure S9. Effects of T_{win} and filtering on the CC value between two events that have been verified to be true repeaters (events No. 1 and No. 3, Figure 3) with single-station (3-channel) data. Notice that station SCYB is not used in this case because of heavy noise contamination. (a) CC determined by T_{win} that is dynamically adjusted for each station. (b)-(d) correspond to the T_{win} of 1.5, 3.0, 4.5, and 6.0 s, respectively.

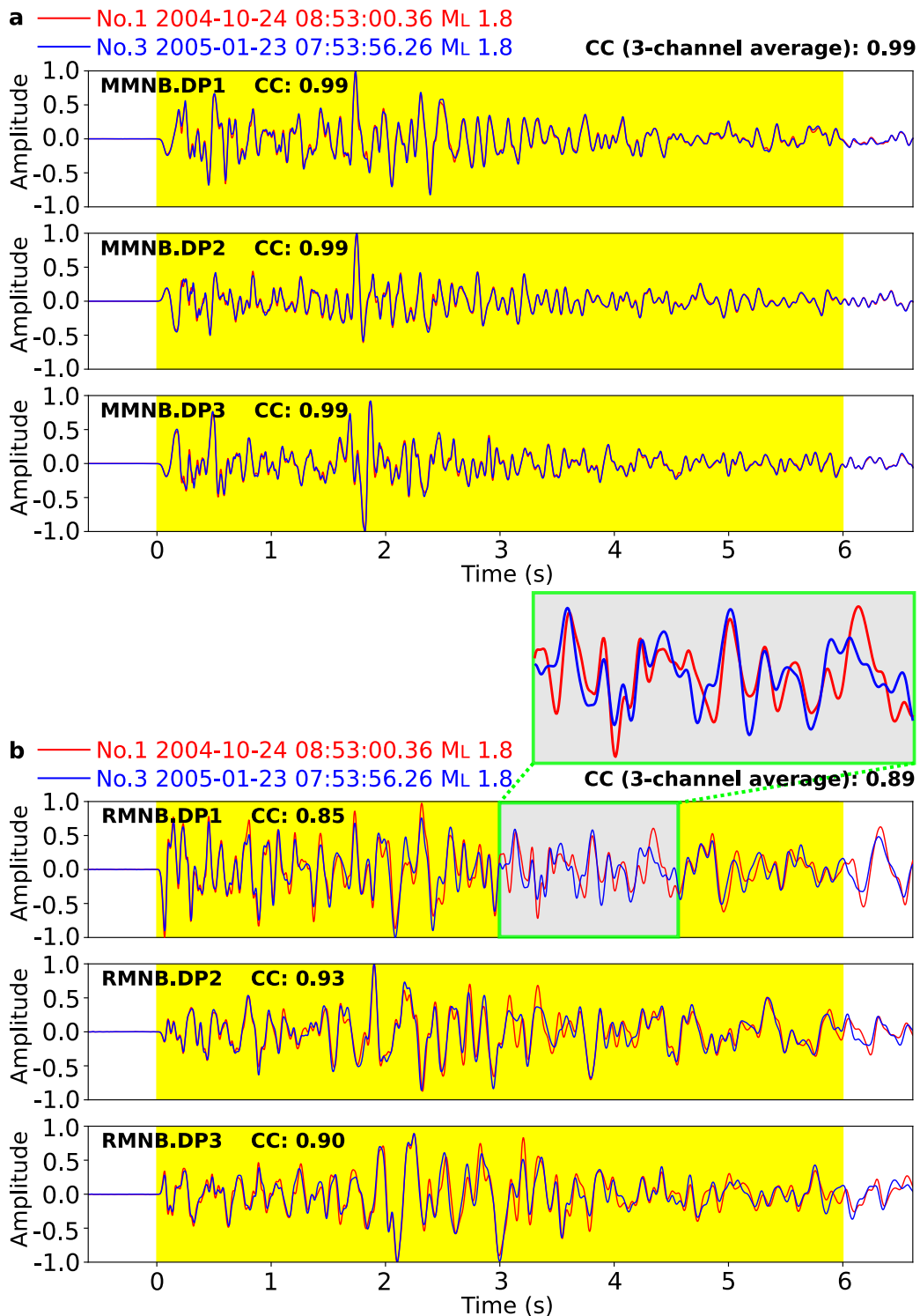


Figure S10. Examples of normalized unfiltered waveforms of two events that have been verified to be true repeaters (events No. 1 and No. 3, Figure 3). (a) Nearly identical waveforms at station MMNB. (b) Waveforms with minor difference at station RMNB. The highlighted segment ($T_{win} = 6.0$ s) is used to calculate the CC value.

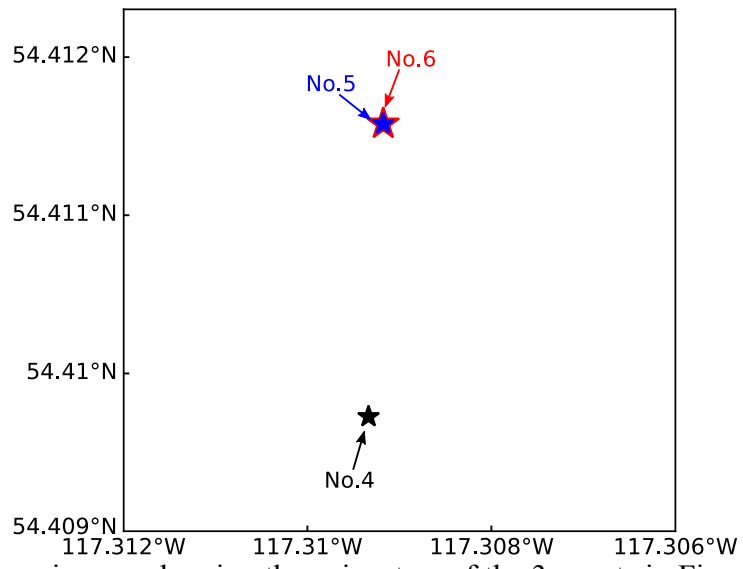


Figure S11. Zoom-in map showing the epicenters of the 3 events in Figure 4.

Table S1. A compiled list of different criteria in identifying repeaters

References	Region	CC Threshold	Additional Criteria/Analysis	Min. Num. of Stations ^{a,b}	Note
Green and Neuberg (2006)	Soufrière Hills Volcano, Montserrat	0.70		1 station (vertical channel)	
Salvagea and Neuberg (2016)	Soufrière Hills Volcano, Montserrat	0.70		1 station (–)	
Yamada et al. (2016)	Hokkaido, Japan	0.70		1 station (three channels)	
Thelen et al. (2010)	Bezymianny Volcano, Russia	0.70/0.80		2 stations (–)	CC = 0.70 for daily detection; CC = 0.80 for merging results from different days
Thelen et al. (2011)	Mount St. Helens (MSH), Washington; Bezymianny Volcano (BV), Russia	0.70/0.80		2 stations for MSH (–); 2 stations for BV (vertical channel)	CC = 0.70 for daily detection; CC = 0.80 for merging results from different days
Rau et al. (2007)	Longitudinal valley fault, Taiwan	0.70/0.85	composite selection criteria (both CC and S-P differential time)	multi-station (vertical channel)	
Chen et al. (2008)	Chihshang fault, TaiWan	0.70/0.85	composite selection criteria (both CC and S-P differential time)	multi-station (vertical channel)	
Buurman et al. (2013)	Redoubt Volcano, south-central Alaska	0.75		1 station (single-channel)	
Schultz et al. (2014)	Alberta, Canada	0.75		1 station (–)	
Cauchie et al. (2020)	Soultz-sous-Forêts, France	0.75	overlap of rupture areas (inter-event distance < the	1 station (vertical channel)	

			sum of event pair radii)		
De Angelis and Henton (2011)	Soufrière Hills Volcano, Montserrat	0.75		3 stations (–)	
Zhang et al. (2005)	South Sandwich Islands region	0.79			
Schaff and Richards (2004)	China	0.80		1 station (BHZ channel)	
Schaff and Richards (2011)	in and near China	0.80		1 station (BHZ channel)	
Buurman and West (2010)	Augustine Volcano, Alaska	0.80		1 station (vertical channel)	
Petersen (2007)	Shishaldin Volcano, Alaska	0.80		1 station (vertical channel)	
Cannata et al. (2013)	Mt. Etna volcano, Italy	0.80		1 station (vertical channel)	
Li and Richards (2003)	South Sandwich Islands region	0.80		1 station (vertical channel)	visually check waveform similarity
Ma and Wu (2013)	Longmen Shan Fault Zone, China	0.80		1 station (three channels)	
Ma et al. (2014)	Longmen Shan Fault Zone, China	0.80		1 station (three channels)	
Nadeau and McEvilly (2004)	San Andreas Fault	0.80	cross-coherence, visual inspection, relocation, arrival time analysis		CC = 0.80 is used for preliminary scanning
Yu (2013)	Tonga-Kermadec-Vanuatu	0.80	entirely overlapping source areas and similar seismic moment	5 stations (vertical channel)	
Li et al. (2007)	Tangshan fault, China	0.85	average recurrence	1 station (–)	

			interval >100 days; internal consistency of travel time picking; relocation	
Zhang et al. (2008)	South Sandwich Islands, Aleutian Islands, Kuril Islands, Tonga–Fiji–Solomon Islands, Bucaramanga earthquake nest	0.90		1 station (vertical channel) visually check waveform similarity
Li et al. (2011)	Longmen Shan fault zone, China	0.90	average recurrence interval >100 days; internal consistency of travel time picking; relative distance < rupture sizes	1 station (–)
Cociani et al. (2010)	Gulf of Corinth, Greece	0.90	inter-event overlap confirmed by relocation and source dimension estimation	1 station (–)
Hayward and Bostock (2017)	Queen Charlotte plate boundary, Canada	0.90	inter-event overlap suggested by coda wave interferometry	1 station (three channels)
Bohnhoff et al. (2017)	Marmara, Turkey	0.90	recurrence time > 30 days; hypocentres ≤ 5 km epicentral distance; magnitude difference $\leq \pm 0.2$	2 stations (vertical channel)

Naoi et al. (2015)	Cooke 4 mine, South Africa	0.90	inter-event separation < half of the rupture radius of the larger event	2 stations (single channel)	
Yamaguchi et al. (2018)	Cooke 4 mine, South Africa	0.90	inter-event separation < half of the rupture radius of the larger event	3 stations (single channel)	
Schmittbuhl et al. (2016)	Main Marmara Fault, Turkey	0.90	confirm overlapping with waveform stretching and spectral analysis	1 station (vertical and horizontal channel)	
Zhao and Peng (2009)	Calaveras fault, California	0.90	magnitude difference < 1; 50% overlapping of the rupture area	3 stations (vertical channel)	CC threshold is the median value at ≥ 3 stations
Meier et al. (2004)	Hellenic subduction zone	0.90		3 stations (-)	
Yao et al. (2017)	Nicoya Peninsula, Costa Rica	0.90	overlap of source area	9 channels	Network-averaged CC
Huang et al. (2020)	Ridgecrest, California	0.90	magnitude difference < 0.5; 50% overlapping of the rupture area; horizontal location error < $0.3 \times$ source radius	6 stations (vertical channel)	
Obana et al. (2003)	western Nankai Trough, Japan	0.93/0.95		2 stations (vertical channel)	
Shirzaei et al. (2013)	Hayward fault, California	0.95	coherency > 0.95	1 station (vertical channel)	
Peng and Ben-Zion (2005)	Karadere-Düzce branch of the North Anatolian Fault, Turkey	0.95			

Igarashi et al. (2003)	northeastern Japan	0.95		2 stations (vertical channel)
Uchida et al. (2003)	northeastern Japan	0.95		2 stations (vertical channel)
Matsuzawa et al. (2004)	east off northern Honshu, Japan	0.95		2 stations (vertical channel)
Kimura et al. (2006)	Kanto, Japan	0.95		2 stations (-)
Igarashi (2010)	Japan	0.95		2 stations (vertical channel)
Yamashita et al. (2012)	southwestern Japan	0.95		2 stations (vertical channel)
Kato and Igarashi (2012)	Tohoku, Japan	0.95		2 stations (-)
Kato et al. (2012)	Tohoku, Japan	0.95		2 stations (-)
Meng et al. (2015)	Northern Chile	0.95		2 stations (vertical channel)
Huang and Meng (2018)	central Chile	0.95	magnitude difference ≤ 0.5 ; stations span a distance > 50 km	2 stations (vertical channel)
Taira et al. (2014)	San Juan Bautista, San Andreas fault	0.95	phase coherency ≥ 0.95	2 stations (vertical channel)
Nishikawa and Ide (2018)	Ibaraki-Oki, Japan	0.95	magnitude difference ≤ 0.5	2 stations (three channels)
Igarashi (2020)	Japan	0.95	composite selection criteria (both CC and S-P differential time)	2 stations (vertical channel)
Matsubara et al. (2005)	northern Japan	0.95		3 stations (vertical channel)
Kato and Nakagawa (2014)	Chile	0.95		4 stations (vertical channel)

Warren-Smith et al. (2018)	New Zealand	0.95	4 stations (-)	
Chaves et al. (2020)	Nicoya Peninsula, Costa Rica	0.95	Multi-station (vertical channel)	Network-averaged CC
Nadeau et al. (1995)	Parkfield, California	0.98		
Nadeau and McEvilly (1999)	Parkfield, California	0.98		
Hatch et al. (2020)	Virginia, Nevada	0.98	4 stations (-)	

^a The minimum number of stations required for a pair of events to be classified as repeaters with the CC value exceeding the threshold value. In this column, the employed channel(s) is given in the brackets if it is explicitly documented in the reference or confirmed by the author, otherwise a dash symbol “-” is denoted.

^b For the cases using data from two or more stations, only Yao et al. (2017) and Chaves et al. (2020) calculate the CC value simultaneously across multiple stations, and then take the average. All others compute the CC value at individual stations separately and claim an event pair to be repeaters if a certain number of stations have the CC values exceeding a given CC threshold.

Table S2. A list of digital filters commonly used in identifying repeaters

Filter	References
No Filter	Warren-Smith et al. (2018)
1–20 Hz	Cannata et al. (2013); Kimura et al. (2006)
1–10 Hz	Li et al. (2007, 2011); Ma and Wu (2013); Ma et al. (2014); Cociani et al. (2010); Schmittbuhl et al. (2016)
1–8 Hz	Matsubara et al. (2005); Meng et al. (2015); Huang and Meng (2018) ; Taira et al. (2014)
0.5–5 Hz	Green and Neuberg (2006); Schaff and Richards (2004, 2011)
1–4 Hz	Igarashi et al. (2003); Igarashi (2010, 2020); Uchida et al. (2003); Matsuzawa et al. (2004); Kato et al. (2012); Meng et al. (2015); Huang and Meng (2018)

Table S3. A list of commonly assumed $\Delta\sigma$ in estimating the ERR

Stress drop	References
3 MPa	Li et al. (2007); Lengliné and Marsan (2009); Schaff and Richards (2011); Shirzaei et al. (2013); Ma et al. (2014); Mesimeri and Karakostas (2018); Huang and Meng (2018); Igarashi (2020)
5 MPa	Li et al. (2011)
10 MPa	Igarashi et al. (2003); Matsuzawa et al. (2004); Uchida and Matsuzawa (2013); Hatakeyama et al. (2017)

References

- Baisch, S., Ceranna, L., & Harjes, H. P. (2008). Earthquake cluster: What can we learn from waveform similarity?. *Bulletin of the Seismological Society of America*, *98*(6), 2806-2814.
- Bao, X., & Eaton, D. W. (2016). Fault activation by hydraulic fracturing in western Canada. *Science*, *354*(6318), 1406-1409.
- Buurman, H., & West, M. E. (2010). Seismic precursors to volcanic explosions during the 2006 eruption of Augustine Volcano. In J. A. Power, M. L. Coombs, & J. T. Freymueller, (Eds.), *The 2006 eruption of Augustine Volcano, Alaska, Professional Paper* (Vol. 1769, chap. 2, pp. 41–57). Washington, DC: U.S. Geological Survey.
- Buurman, H., West, M. E., & Thompson, G. (2013). The seismicity of the 2009 Redoubt eruption. *Journal of Volcanology and Geothermal Research*, *259*, 16-30.
- Cannata, A., Alparone, S., & Ursino, A. (2013). Repeating volcano-tectonic earthquakes at Mt. Etna volcano (Sicily, Italy) during 1999–2009. *Gondwana research*, *24*(3-4), 1223-1236.
- Cauchie, L., Lengliné, O., & Schmittbuhl, J. (2020). Seismic asperity size evolution during fluid injection: case study of the 1993 Soultz-sous-Forêts injection. *Geophysical Journal International*, *221*(2), 968-980.
- Chaves, E. J., Schwartz, S. Y., & Abercrombie, R. E. (2020). Repeating earthquakes record fault weakening and healing in areas of megathrust postseismic slip. *Science advances*, *6*(32), eaaz9317.
- Chen, K. H., Nadeau, R. M., & Rau, R. J. (2008). Characteristic repeating earthquakes in an arc-continent collision boundary zone: The Chihshang fault of eastern Taiwan. *Earth and Planetary Science Letters*, *276*(3-4), 262-272.
- Cociani, L., Bean, C. J., Lyon-Caen, H., Pacchiani, F., & Deschamps, A. (2010). Coseismic velocity variations caused by static stress changes associated with the 2001 Mw= 4.3 Agios Ioanis earthquake in the Gulf of Corinth, Greece. *Journal of Geophysical Research: Solid Earth*, *115*(B7).
- De Angelis, S., & Henton, S. M. (2011). On the feasibility of magma fracture within volcanic conduits: constraints from earthquake data and empirical modelling of magma viscosity. *Geophysical Research Letters*, *38*(19).
- Green, D. N., & Neuberg, J. (2006). Waveform classification of volcanic low-frequency earthquake swarms and its implication at Soufrière Hills Volcano, Montserrat. *Journal of Volcanology and Geothermal Research*, *153*(1-2), 51-63.
- Hatakeyama, N., Uchida, N., Matsuzawa, T., & Nakamura, W. (2017). Emergence and disappearance of interplate repeating earthquakes following the 2011 M9.0 Tohoku-oki earthquake: Slip behavior transition between seismic and aseismic depending on the loading rate. *Journal of Geophysical Research: Solid Earth*, *122*(7), 5160-5180.
- Hatch, R. L., Abercrombie, R. E., Ruhl, C. J., & Smith, K. D. (2020). Evidence of Aseismic and Fluid-Driven Processes in a Small Complex Seismic Swarm Near Virginia City, Nevada. *Geophysical Research Letters*, *47*(4), e2019GL085477.

- Huang, H., & Meng, L. (2018). Slow unlocking processes preceding the 2015 Mw 8.4 Illapel, Chile, earthquake. *Geophysical Research Letters*, 45(9), 3914-3922.
- Huang, H., Meng, L., Bürgmann, R., Wang, W., & Wang, K. (2020). Spatio-temporal foreshock evolution of the 2019 M 6.4 and M 7.1 Ridgecrest, California earthquakes. *Earth and Planetary Science Letters*, 551, 116582.
- Igarashi, T. (2010). Spatial changes of inter-plate coupling inferred from sequences of small repeating earthquakes in Japan. *Geophysical research letters*, 37(20).
- Igarashi, T. (2020). Catalog of small repeating earthquakes for the Japanese Islands. *Earth, Planets and Space*, 72, 1-8.
- Igarashi, T., Matsuzawa, T., & Hasegawa, A. (2003). Repeating earthquakes and interplate aseismic slip in the northeastern Japan subduction zone. *Journal of Geophysical Research: Solid Earth*, 108(B5).
- Kato, A., & Igarashi, T. (2012). Regional extent of the large coseismic slip zone of the 2011 Mw 9.0 Tohoku-Oki earthquake delineated by on-fault aftershocks. *Geophysical Research Letters*, 39(15).
- Kimura, H., Kasahara, K., Igarashi, T., & Hirata, N. (2006). Repeating earthquake activities associated with the Philippine Sea plate subduction in the Kanto district, central Japan: A new plate configuration revealed by interplate aseismic slips. *Tectonophysics*, 417(1-2), 101-118.
- Kraft, T., & Deichmann, N. (2014). High-precision relocation and focal mechanism of the injection-induced seismicity at the Basel EGS. *Geothermics*, 52, 59-73.
- Lengliné, O., & Marsan, D. (2009). Inferring the coseismic and postseismic stress changes caused by the 2004 Mw= 6 Parkfield earthquake from variations of recurrence times of microearthquakes. *Journal of Geophysical Research: Solid Earth*, 114(B10).
- Li, L., Niu, F., Chen, Q. F., Su, J., & He, J. (2017). Post-seismic velocity changes along the 2008 M 7.9 Wenchuan earthquake rupture zone revealed by S coda of repeating events. *Geophysical Journal International*, 208(2), 1237-1249.
- Ma, S. (2010). Focal depth determination for moderate and small earthquakes by modeling regional depth phases sPg, sPmP, and sPn. *Bulletin of the Seismological Society of America*, 100(3), 1073-1088.
- Ma, S., & Atkinson, G. M. (2006). Focal depths for small to moderate earthquakes ($m \geq 2.8$) in Western Quebec, Southern Ontario, and Northern New York. *Bulletin of the Seismological Society of America*, 96(2), 609-623.
- Ma, X. J., & Wu, Z. L. (2013). 'Negative repeating doublets' in an aftershock sequence. *Earth, Planets and Space*, 65(8), 923-927.
- Ma, X., Wu, Z., & Jiang, C. (2014). 'Repeating earthquakes' associated with the WFSD-1 drilling site. *Tectonophysics*, 619, 44-50.

- Matsubara, M., Yagi, Y., & Obara, K. (2005). Plate boundary slip associated with the 2003 Off-Tokachi earthquake based on small repeating earthquake data. *Geophysical Research Letters*, 32(8).
- Matsuzawa, T., Uchida, N., Igarashi, T., Okada, T., & Hasegawa, A. (2004). Repeating earthquakes and quasi-static slip on the plate boundary east off northern Honshu, Japan. *Earth, planets and space*, 56(8), 803-811.
- Meng, L., Huang, H., Bürgmann, R., Ampuero, J. P., & Strader, A. (2015). Dual megathrust slip behaviors of the 2014 Iquique earthquake sequence. *Earth and Planetary Science Letters*, 411, 177-187.
- Mesimeri, M., & Karakostas, V. (2018). Repeating earthquakes in western Corinth Gulf (Greece): implications for aseismic slip near locked faults. *Geophysical Journal International*, 215(1), 659-676.
- Myhill, R., McKenzie, D., & Priestley, K. (2011). The distribution of earthquake multiplets beneath the southwest Pacific. *Earth and Planetary Science Letters*, 301(1-2), 87-97.
- Nadeau, R. M., & McEvilly, T. V. (1999). Fault slip rates at depth from recurrence intervals of repeating microearthquakes. *Science*, 285(5428), 718-721.
- Nadeau, R. M., & McEvilly, T. V. (2004). Periodic pulsing of characteristic microearthquakes on the San Andreas fault. *Science*, 303(5655), 220-222.
- Nadeau, R. M., Foxall, W., & McEvilly, T. V. (1995). Clustering and periodic recurrence of microearthquakes on the San Andreas fault at Parkfield, California. *Science*, 267(5197), 503-507.
- Naoi, M., Nakatani, M., Igarashi, T., Otsuki, K., Yabe, Y., Kgarume, T., ... & Moriya, H. (2015). Unexpectedly frequent occurrence of very small repeating earthquakes ($-5.1 \leq MW \leq -3.6$) in a South African gold mine: implications for monitoring intraplate faults. *Journal of Geophysical Research: Solid Earth*, 120(12), 8478-8493.
- Nishikawa, T., & Ide, S. (2018). Recurring slow slip events and earthquake nucleation in the source region of the M 7 Ibaraki-Oki earthquakes revealed by earthquake swarm and foreshock activity. *Journal of Geophysical Research: Solid Earth*, 123(9), 7950-7968.
- Obana, K., Kodaira, S., Kaneda, Y., Mochizuki, K., Shinohara, M., & Suyehiro, K. (2003). Microseismicity at the seaward updip limit of the western Nankai Trough seismogenic zone. *Journal of Geophysical Research: Solid Earth*, 108(B10).
- Peng, Z., & Ben-Zion, Y. (2005). Spatiotemporal variations of crustal anisotropy from similar events in aftershocks of the 1999 M 7.4 Izmit and M 7.1 Düzce, Turkey, earthquake sequences. *Geophysical Journal International*, 160(3), 1027-1043.
- Petersen, T. (2007). Swarms of repeating long-period earthquakes at Shishaldin Volcano, Alaska, 2001–2004. *Journal of Volcanology and Geothermal Research*, 166(3-4), 177-192.

- Rau, R. J., Chen, K. H., & Ching, K. E. (2007). Repeating earthquakes and seismic potential along the northern Longitudinal Valley fault of eastern Taiwan. *Geophysical research letters*, 34(24).
- Robinson, D. J., Sambridge, M., & Snieder, R. (2011). A probabilistic approach for estimating the separation between a pair of earthquakes directly from their coda waves. *Journal of Geophysical Research: Solid Earth*, 116(B4).
- Salvage, R. O., & Neuberg, J. W. (2016). Using a cross correlation technique to refine the accuracy of the Failure Forecast Method: Application to Soufrière Hills volcano, Montserrat. *Journal of Volcanology and Geothermal Research*, 324, 118-133.
- Schmitzbuhl, J., Karabulut, H., Lengliné, O., & Bouchon, M. (2016). Long-lasting seismic repeaters in the Central basin of the Main Marmara fault. *Geophysical Research Letters*, 43(18), 9527-9534.
- Schultz, R., Stern, V., & Gu, Y. J. (2014). An investigation of seismicity clustered near the Cordell Field, west central Alberta, and its relation to a nearby disposal well. *Journal of Geophysical Research: Solid Earth*, 119(4), 3410-3423.
- Schultz, R., Wang, R., Gu, Y. J., Haug, K., & Atkinson, G. (2017). A seismological overview of the induced earthquakes in the Duvernay play near Fox Creek, Alberta. *Journal of Geophysical Research: Solid Earth*, 122(1), 492-505.
- Shearer, P. M. (1997). Improving local earthquake locations using the L1 norm and waveform cross correlation: Application to the Whittier Narrows, California, aftershock sequence. *Journal of Geophysical Research: Solid Earth*, 102(B4), 8269-8283.
- Shearer, P. M. (2009). *Introduction to seismology*. Cambridge university press.
- Shirzaei, M., Bürgmann, R., & Taira, T. A. (2013). Implications of recent asperity failures and aseismic creep for time-dependent earthquake hazard on the Hayward fault. *Earth and Planetary Science Letters*, 371, 59-66.
- Snieder, R., & Vrijlandt, M. (2005). Constraining the source separation with coda wave interferometry: Theory and application to earthquake doublets in the Hayward fault, California. *Journal of Geophysical Research: Solid Earth*, 110(B4).
- Taira, T. A., Bürgmann, R., Nadeau, R. M., & Dreger, D. S. (2014). Variability of fault slip behavior along the San Andreas Fault in the San Juan Bautista Region. *Journal of Geophysical Research: Solid Earth*, 119(12), 8827-8844.
- Thelen, W., Malone, S., & West, M. (2011). Multiplets: Their behavior and utility at dacitic and andesitic volcanic centers. *Journal of Geophysical Research: Solid Earth*, 116(B8).
- Thelen, W., West, M., & Senyukov, S. (2010). Seismic characterization of the fall 2007 eruptive sequence at Bezymianny Volcano, Russia. *Journal of Volcanology and Geothermal Research*, 194(4), 201-213.
- Trugman, D. T., & Shearer, P. M. (2017). GrowClust: A hierarchical clustering algorithm for relative earthquake relocation, with application to the Spanish Springs and

- Sheldon, Nevada, earthquake sequences. *Seismological Research Letters*, 88(2A), 379-391.
- Uchida, N., & Matsuzawa, T. (2013). Pre-and postseismic slow slip surrounding the 2011 Tohoku-oki earthquake rupture. *Earth and Planetary Science Letters*, 374, 81-91.
- Uchida, N., Matsuzawa, T., Hasegawa, A., & Igarashi, T. (2003). Interplate quasi-static slip off Sanriku, NE Japan, estimated from repeating earthquakes. *Geophysical Research Letters*, 30(15).
- Wang, R., Gu, Y. J., Schultz, R., Zhang, M., & Kim, A. (2017). Source characteristics and geological implications of the January 2016 induced earthquake swarm near Crooked Lake, Alberta. *Geophysical Journal International*, 210(2), 979-988.
- Warren-Smith, E., Fry, B., Kaneko, Y., & Chamberlain, C. J. (2018). Foreshocks and delayed triggering of the 2016 MW7. 1 Te Araroa earthquake and dynamic reinvigoration of its aftershock sequence by the MW7. 8 Kaikōura earthquake, New Zealand. *Earth and Planetary Science Letters*, 482, 265-276.
- Yamaguchi, J., Naoi, M., Nakatani, M., Moriya, H., Igarashi, T., Murakami, O., ... & Ogasawara, H. (2018). Emergence and disappearance of very small repeating earthquakes on a geological fault in a gold mine in South Africa. *Tectonophysics*, 747, 318-326.
- Yamashita, Y., Shimizu, H., & Goto, K. (2012). Small repeating earthquake activity, interplate quasi-static slip, and interplate coupling in the Hyuga-nada, southwestern Japan subduction zone. *Geophysical research letters*, 39(8).
- Zhang, J., Song, X., Li, Y., Richards, P. G., Sun, X., & Waldhauser, F. (2005). Inner core differential motion confirmed by earthquake waveform doublets. *Science*, 309(5739), 1357-1360.
- Zhao, P., & Zhigang, P. (2009). Depth extent of damage zones around the central Calaveras fault from waveform analysis of repeating earthquakes. *Geophysical Journal International*, 179(3), 1817-1830.